CHAPTER III

Dielectric Studies in the Vicinity of the A-C* Transition

3.1 Introduction

Experimental studies on liquid crystals using dielectric[1,2] measurements as a probe has yielded valuable data which are of great significance from both the fundamental and applied aspects. Through tliese studies it has been possible to extract information regarding the dipolar ordering in the nematic,[3] polymorphic forms of smectic A and the smectic C phases[4,5] and the role played by different material parameters.

The shape anisotropy - length to breadth ratio ~ 5 - of the molecules manifests itself in the dielectric permittivity of liquid crystals. There are two principal dielectric constants parallel ($\epsilon_{\|}$) and perpendicular ($\epsilon_{\perp}$) to the director. $\epsilon_{\|}$ exhibits a relaxation in tlie radio frequency region (associated with the flipping of the molecules around their short axis), while $\epsilon_{\perp}$ shows a relaxation in the microwave region representing the rotation of tlie molecules around their long axis. In addition, of course, there will be the very high frequency contribution due to the different parts of the molecules with their own internal degrees of rotation. Thus the measurement of

dielectric constant provitles a powerful tool in understanding the static and dynamic behaviour of tlie system. The importance of these studies in ferroelectric liquid crystalline materials lies in tlie fact that it relates macroscopic properties like spontaneous polarization to microscopic parameters like the dipole moment of the molecule.

In this chapter we present results of detailed investigations on the influence of various parameters on the dielectric properties in FLCs.

It may be recalled that tlie A – C* transition is not driven by tlie spontaneous polarisation P_s, but the molecular tilt θ.[6] But as the two are effectively coupled, P_s also goes to zero at the transition to A phase. Hence in analogy with the paraelectric-ferroelectric transition in solid ferroelectrics tlie transition temperature T_c at which P_s goes to zero is referred to as the Curie point. In fact dielectric measurements near the $A - C^*$ transition reveal some of tlie features exhibited by the solid ferroelectrics (wliere P_s is the primary order parameter) near tlie Curie point.

Earlier dielectric studies[7–20] on FLCs have established the following:

1. Just like their achiral analogues, there is a low frequency relaxation mode associated with the flipping of tlie molecules around their short axis. This is observed as a dispersion in the $\epsilon_{\|}$ the dielectric constant along the layer normal direction.

2. $\epsilon_{\perp}$ shows two low frequency director relaxation modes, viz., the soft mode (SM) and the Goldstone mode (GM). The former appears both in C* and the A phases close to T_c, but the latter exists only in tlie C^* phase.

Several stuclies have been made to characterise these modes by measuring $\epsilon_{\perp}$ as a function of temperature and frequency,[7–12] applied field strength,[13] thickness of

the sample[15,16] and DC bias field [18,20] across the $A - C^*$ transition. However there are hardly any reports on the effect of the magnitude of P_s, alkyl chain length, etc., on the static and dispersion behaviour of $\epsilon_\perp$. The studies presented in this chapter describes the influence of these parameters. Further the results are discussed in the light of the predictions of the generalized Landau model[21,22] which has been quite successful in explaining the behaviour of many other ferroelectric properties.

Experiments carried out on a homologues series of compounds help in understanding the role played by the elastic torque and the associated viscosity in determining tlie relaxation parameters. A novel method of analysing tlie SM results using which two important Landau coefficients can be calculated, is also presented. We will start with a general introduction to tlie dielectric studies in FLCs.

3.1.1 Dielectric spectra of ferroelectric liquid crystals

As mentioned earlier the behaviour of $\epsilon_\parallel$, the dielectric constant parallel to the director, is very similar in both chiral and achiral systems. On the other hand, the transverse dielectric constant $\epsilon_\perp$ exhibits drastically different behaviour in chiral systems. Figure 3.1 is a schematic representation[23] of the different types of relaxations seen in $\epsilon_\parallel$ and $\epsilon_\perp$ for a FLC. $\epsilon_\parallel$ has ttvo high frequency relaxations[2'] - one due to the molecular rotation around the short axis (frequency range 10^5-10^7 Hz) and the other due to the molecular reorientation around the short axis (frequency range 10^8 - 10^{10} Hz). For $\epsilon_\perp$ there is one dispersion due to molecular rotations around the long axis (frequency range 10^8-10^{10} Hz) and the other due to the intramolecular rotation at still higher frequency range. At lower frequencies (frequency range of 10^2-10^6 Hz) the spectra contains two more modes identified to he director relaxation modes. These are referred to as soft mode (SM) arid tlie Coldstone mode (GM)

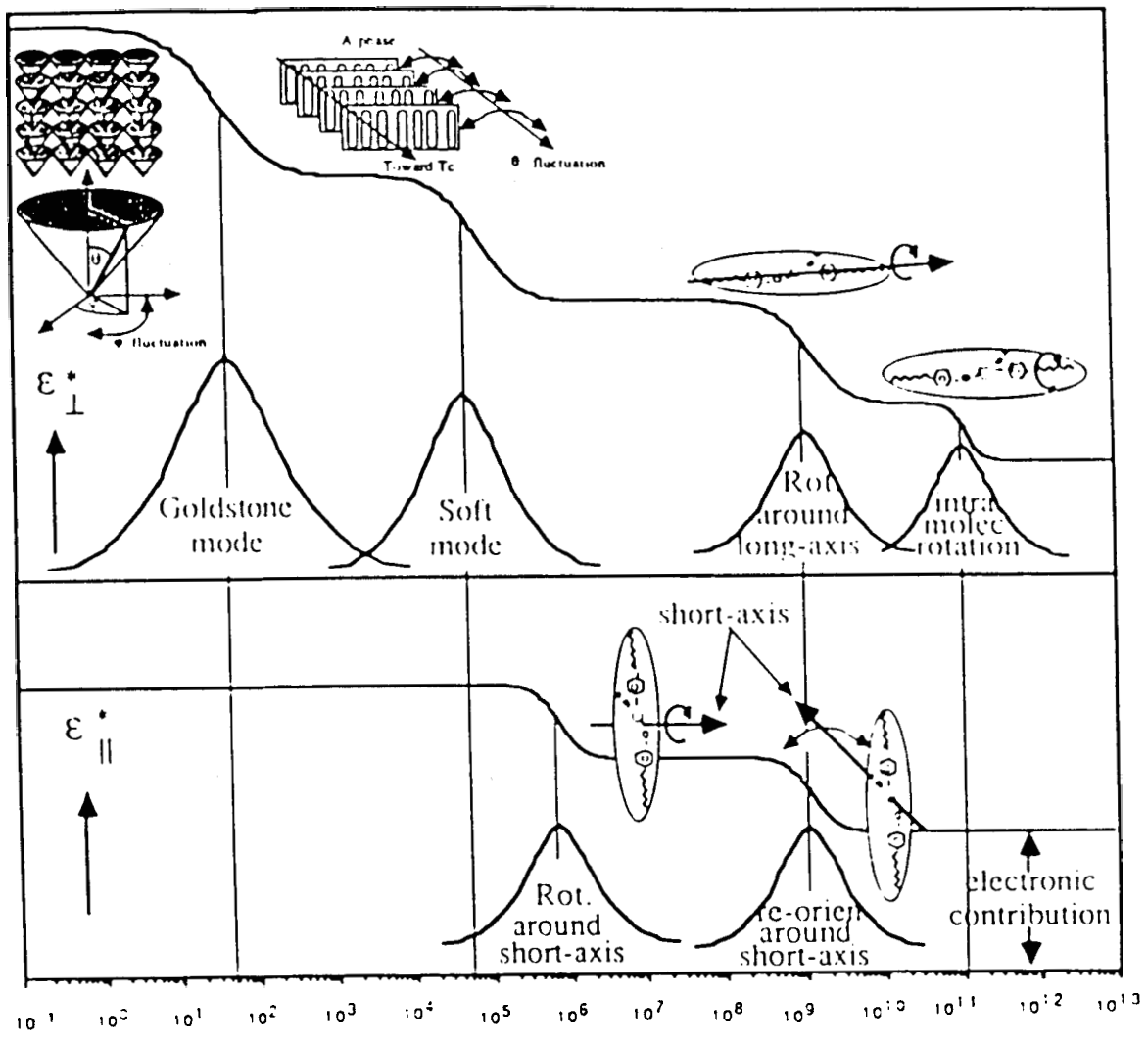

Fig.3.1. Frequency dependence of the perpendicular, $\epsilon_{\perp}$, and parallel, $\epsilon_{||}$, components of the complex dielectric permittivity in the A and C* phases, connected to the collective and non-collective molecular mechanisms (From ref.23).

relaxations.[10,25] While both the modes are present in C* pliase only SM is observed in the A phase.

The characteristic feature of FLC is the helical distribution of the permanent dipoles of the molecules. When a measuring electric field is applied in a direction parallel to the layers anti perpendicular to the helix, the field will disturb the helix in two ways. First, it induces an additional tilt (due to the electroclinic effect[26] described in Chapter I) and thus changes the amplitude of tlie tilt. Secondly, the azimuthal direction of the tilt changes (thus changing the pliase) enabling tlie dipole to orient in the field direction. Hence tlie disturbance of the equilibrium order parameters due to an applied electric field can be divided into two parts; amplitude and phase parts.[27] As we shall see presently these are denoted as soft mode and Goldstone mode respectively.

Soft mode

Raman and Nedungadi[28] were the first to observe the existence of soft modes in a structural phase transition. Using Raman scattering, they found that the frequency of a totally symmetric optical phonon decreases (softens) as the $\alpha \rightarrow \beta$ transition in quartz is approached. In a similar fashion in FLCs, the elastic forces controlling the tilt fluctuations become soft as the $A-C^*$transition is approached from the A phase, owing to this the amplitude of the tilt fluctuation (see Fig.3.2a) increases drastically and its susceptibility diverges at T_c and its frequency tends to zero. For this reason this tilt amplitude fluctuation mode is called the soft mode (SM). The SM exists in non-cliiral liquid crystalline system also, however tlie amplitude would be very small. Since near T_c the molecules are susceptible for tilt fluctuations even a weak electric field applied in a direction perpendicular to the director can easily perturb the equilibrium director orientation. For non-chiral smectic A phase tlie induced

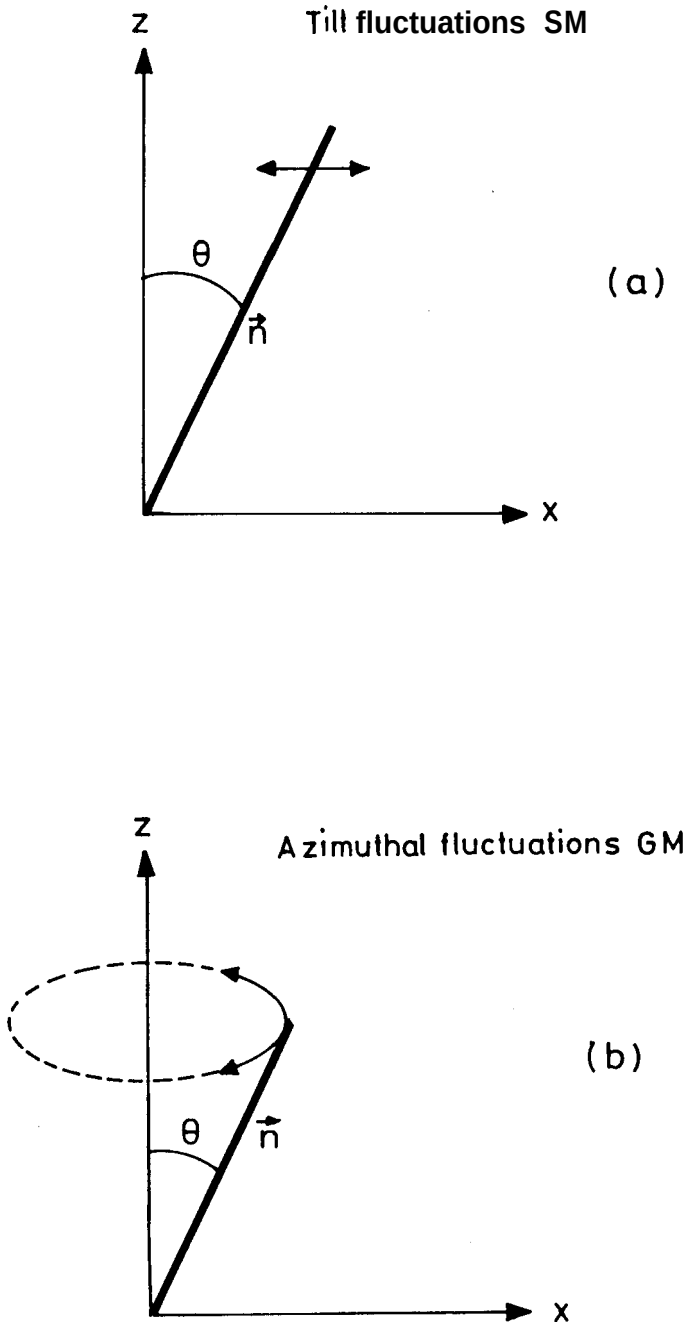

Fig.3.2. Schematic diagram illustrating the director fluctuation rnodes in the C* phase: (a) Soft mode, (b) Goldstone mode.

dipole moment due to the applied field is too small to be detected by dielectric measurements. However, the tilt fluctuations in these systems can be studied by light scattering.[29] In FLCs the chirality enhances the induced dipole moment due to the electroclinic effect thus permitting the study of *SM* by dielectric methods.[23]

Goldstone Mode

One of tlie characteristic features of $A - C^*$ transition is that C* phase has lower symmetry than the high temperature *A* phase, i.e., $A - C^*$ transition involves the breaking of a continuous symmetry group. According to the Goldstone theorem[30] a symmetry recovering order fluctuation mode - tlie Goldstone mode - will appear below T_c in addition to the soft mode. In A phase, the molecules are along tlie layer normal and hence the phase is uniaxial. In the C* phase the molecules are tilted which breaks tlie uniaxial symmetry of the molecule and makes it biaxial. However the existence of the helicoidal structure allows the C* phase to recover tlie macroscopic uniaxial symmetry. As such the symmetry recovering relaxation mode - referred to as tlie Goldstone mode (GM) should be related to the helix or equivalently to the phase changes of the tilt order parameter (see Fig. 3.2b). When an AC electric field is applied, tlie helix gets distorted and tlie process of tlie restoring of the distorted helix is described by the relaxation of GM.[10] Owing to the macroscopic dimension of the helix ($\sim \mu m$), the *GM* relaxation frequency turns out to be quite low ($10^2 \sim 10^3$ Hz) for the same reason tlie strength of GM is large.

3.1.2 Thermodynamic model

Attempts have been made to explain various thermodynamic properties of Sm C* phase in terms of phenomenological models[21,22,31] involving a Landau free energy expansion. These models are based on tlie idea that the free energy can be expanded in terms of a Taylor series in the order parameter reflecting the symmetry properties

of the medium. It is important to note that the tilt of the molecules drives the A–C* transition, and, as pointed out in earlier chapters, the appearance of P_s, which arises only as an associated effect, is the secondary order parameter.

Just as in tlie non-chiral C phase the tilt is described by a complex order parameter which can be resolved into a niagnitude part and a phase part represented by the polar angle θ arid the azimuthal angle ϕ respectively. Geometrically, the tilt vector $\vec{\xi} = (\vec{\xi_1}, \vec{\xi_2})$ is tlie projection of tlie director $\vec{n}$ on to the smectic planes. The existence of non-zero tilt breaks the axial symmetry around the long molecular axis. If the substance is chiral this induces an ill-plane polarization $\vec{P} = (\vec{P_x}, \vec{P_y})$ perpendicular to the tilt direction (see Fig.3.3). (Here P_x and P_y are the orthogonal components of $\vec{P}$ in the smectic plane.) For a general description of the C* phase, along with these order parameter terms one has to include terms accounting for the helicoidal structure of the phase. As there are two order parameters one of them being secondary, it is natural to include coupling terms between them. Two sirnplest types of coupling terms are:

Piezoelectric.

The lowest order coupling term of this type is given by $C(P_x\xi_2 - P_y\xi_1)$, C is called the bilinear coupling constant.

Flexoelectric.

At the molecular level, flexoelectricity exists clue to special shapes of the constituent molecules. But in tlie C^* phase this is caused by the macroscopic helicoidal structure. The distortion of the director gives rise to contribution of tlie type $\mu(P_x\frac{\partial\xi_1}{\partial z} + P_y\frac{\partial\xi_2}{\partial z})$, μ being flexoelectric coefficient. Notice that this term vanishes for an unwound sample.

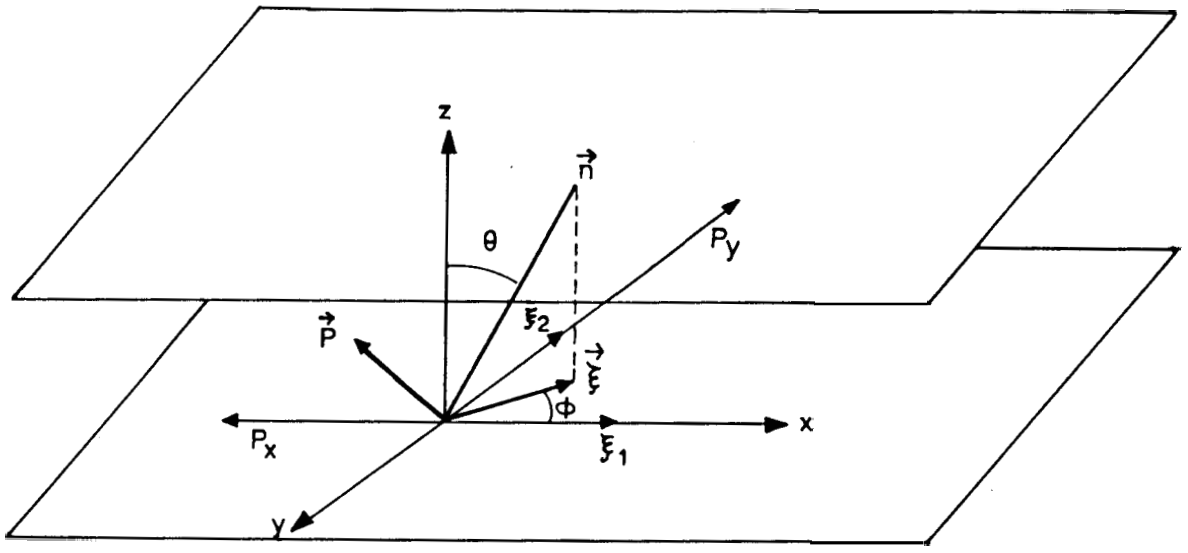

Fig.3.3. The components of the order parameter $\vec{\xi}$ and $\vec{P_s}$.

Putting together the various terms, the free energy expansion can be written as[3]

$$g(z) = \frac{1}{2}a(\xi_1^2+\xi_2^2)+\frac{1}{4}b(\xi_1^2+\xi_2^2)^2-\Lambda(\xi_1\frac{d\xi_2}{dz}-\xi_2\frac{d\xi_1}{dz})+\frac{1}{2}K_3\left[\left(\frac{d\xi_1}{dz}\right)^2+\left(\frac{d\xi_2}{dz}\right)^2\right]$$

$$+\frac{1}{2\epsilon}\left(P_x^2+P_y^2\right)-\mu\left(P_x\frac{d\xi_1}{dz}+P_y\frac{d\xi_2}{dz}\right)+C(P_x\xi_2-P_y\xi_1) \qquad (3.1)$$

where a and b are the usual Landau coefficients and it is assumed that 'a' is the only temperature dependent coefficient with $a = \alpha(T - T_o)$, where T_o is the transition temperature for the racemic mixtures (without helix arid $A = C = 0$), K_3 an elastic constant, A the Lifshitz invariant, ϵ is the high temperature dielectric constant.

To simplify eqn. (3.1) the values of ξ_1, ξ_2 and P_x, P_y have to he found. Figure **3.3** shows the components ξ_1, ξ_2 and P_x, P_y. For small tilt angles,

$$\xi_1 = \theta\cos\phi \quad \text{and} \quad \xi_2 = \theta\sin\phi$$

where $\phi = \phi(z)$ is the azimuthal angle determining tlie orientation of the director $\vec{n}$ with respect to z-axis, i.e., normal to the srnectic layers. If q is the wavevector of the helix then $\phi = qz$. Similarly, $P_x = -P_o\sin\phi$ and $P_y = P_o\cos\phi$ are the components of P_s along x and y axes. Substituting the values of ξ_1, ξ_2 and P_x, P_y in eqn.(3.1), we get

$$g(z) = g_o + \frac{1}{2}a\theta^2+\frac{1}{4}b\theta^4-\Lambda q\theta^2+\frac{1}{2}K_3q^2\theta^2+\frac{1}{2\epsilon}P^2-\mu Pq\theta-CP\theta \qquad (3.2)$$

Expressions for the A–C*transition temperature T_c, the temperature dependence of the tilt angle 0, pitch of the helix and polarisation P_s can he obtained by minimising eqn. (3.2) with respect to θ, I and q.

$$T_c = T_o+\frac{1}{2}[\epsilon C^2+(K_3-\epsilon\mu^2)q^2] \qquad (3.3)$$

$$\theta = [\frac{\alpha}{b}(T_c - T)]^{1/2} \qquad (3.4)$$

$$p = \frac{2\pi}{q} = 2\pi \frac{K_3 - \epsilon\mu^2}{\Lambda + \epsilon\mu C} \tag{3.5}$$

$$P_s = \epsilon(\mu q + C)\theta \tag{3.6}$$

Since all the quantities on the RHS of (3.5) are constants pitch p and hence the ratio P_s/θ from **(3.6)** are independent **of** temperature. This means that the coupling between P_s and θ is strictly linear. Contrary to this, experiments showed that P_s/θ ratio is weakly dependent on temperature away from T_c but has a precipitous drop near it. The temperature dependence of helical pitch is also seen to have an anamalous variation close to T_c. In orcler to explain these factors Carlsson etal., [21] liave proposed a more generalized mean field (GMF) model which included a 6th order term in tilt and a biquadratic coupling term. Then eqn. **(3.2)** becomes

$$g(z) = \frac{1}{2}a\theta^2 + \frac{1}{4}b\theta^4 + \frac{1}{6}c\theta^6 - \Lambda q\theta^2 + \frac{1}{2}K_3q^2\theta^2 + \frac{1}{2\epsilon}P^2 - \mu qP\theta$$

$$-CP\theta - \frac{1}{2}\Omega P^2\theta^2 + \frac{1}{4}\eta P^4 - dq\theta^4 \tag{3.7}$$

Here ***c*** is the Landau coefficient of the 6th order term, Ω tlie biquadratic coupling coefficient, d the higher order Lifshitz invariant included to account for the anomaly in the temperature variation of pitch. The predictions of the generalised model liave found to he in good agreement with tlie experimentally observed features. Now let us see what this model expects for the thermal variation of SM and GM in tlie A and C* phases.[32,33,17]

In smectic A phase,

$$\epsilon_o\Delta\epsilon_s = \frac{\epsilon_o^2\epsilon^2C^2}{[a(T - T_c) + (K_3 - \epsilon\mu^2)q_o^2]} \tag{3.8}$$

$$f_s = \frac{a(T - T_c) + (K_3 - \epsilon\mu^2)q_o^2}{2\pi\eta_{S_A}} \tag{3.9}$$

In smectic C phase,*

For SM

$$\epsilon_o \Delta\epsilon_s = \frac{\epsilon_o^2 \epsilon^2 C^2}{2a(T - T_c) + (K_3 - \epsilon\mu^2)q_o^2} \tag{3.10}$$

$$f_s = \frac{a(T - T_c) + (K_3 - \epsilon\mu^2)q_o^2}{2\pi\eta_S} \tag{3.11}$$

For GM

$$\epsilon_o \Delta\epsilon_G = \frac{1}{2K_3}\left(\frac{P}{q\theta}\right)^2 \tag{3.12}$$

$$f_G = \frac{K_3 q^2}{2\pi\gamma_G} \tag{3.13}$$

In the same paper[32] the authors present a few theoretically expected curves in terms of a dimensionless parameter β where $\beta = \frac{\eta^{1/2}\tilde{C}\tilde{\epsilon}}{\Omega^{1/2}}$ the value of β shows the importance of the biquadratic coupling term Ω. Larger the value of β smaller will be Ω. And β=1 corresponds to the classical case. β is expressed in terms of P_s and θ as

$$\tilde{P}^3 + (1 - \tilde{\theta}^2)\tilde{P} - \beta\tilde{\theta} = 0 \tag{3.14}$$

where $\tilde{P} = P/P^*, \tilde{\theta} = \theta/\theta^*$ and P* and θ^* are the normalising constants. We have

used this equation to evaluate the value of β (see results section). The theoretical plots of $\Delta\epsilon_G$, f_G, and f_s for different values of β are shown in figures 4.4a and 4.4b. At a later stage we compare our data with these theoretical curves.

3.2 Experimental

The experimental set up consists of the sample cell, temperature controlled heater and tlie dielectric measuring set up which includes an impedance analyses and a microcomputer.

3.2.1 Sample cell and alignment of the sample

Tlie method of preparations of the sample cell was exactly similar to the one described in Chapter II. The combined effect of polymer coating and magnetic field (2.4T) applied, along the rubbing direction, while cooling tlie sample from isotropic to *A* phase, was utilized to obtain uniform planar alignment of the samples.

A detailed description of the heater assembly and the temperature control and measurement system is given in Chapter II. Since the frequcricy sweep in tlie dispersion studies took about. 2 minutes, it was necessary to keep the temperature constant over this period. The large thermal capacity of the system enabled to keep the temperature constant at any desired value to wit hin $\pm$ 5 mK.

3.2.2 Measurement of dielectric constant

Tlie dielectric constants were determined by measuring the sample capacitance and dielectric loss factor. A versatile variable frequency Impedance Analyser (Hewlett Packard 3192A) with a measuring frequency range of 5 Hz - 13 MHz was employed for this purpose. In fact tliis instrument can be used to measure as many as eleven

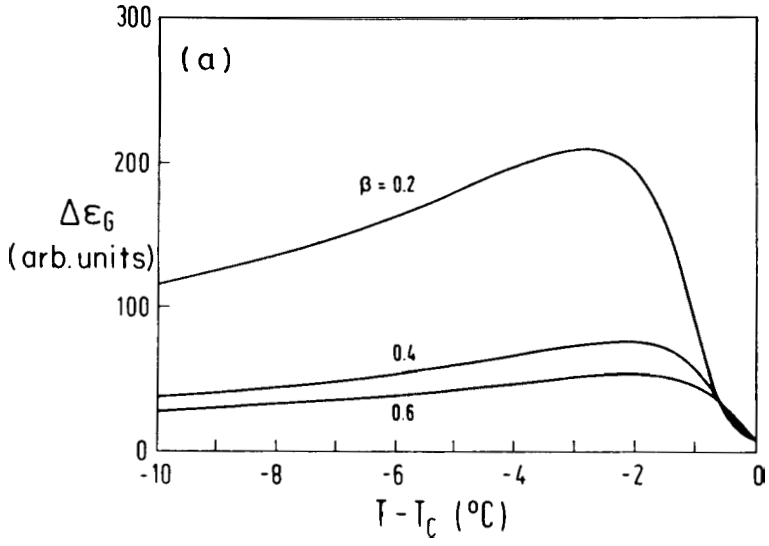

Fig.3.4a. Theoretical plot of $\Delta\epsilon_G$ versus temperature for different values of β (from Ref. 32).

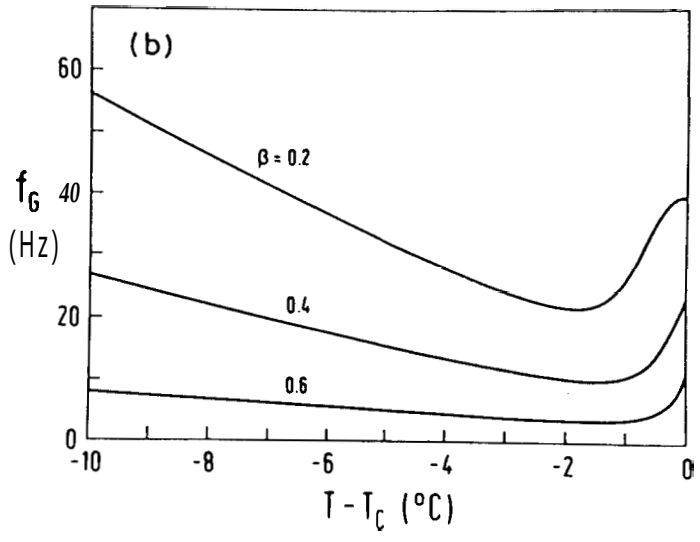

Fig.3.4b. Theoretical plot of f_G versus temperature for different values of β (from Ref.32).

impedance associated parameters such as capacitance C, conductance G, susceptance B, dissipation or dielectric loss factor D, etc., with a basic accuracy of 0.1% throughout the range of measurement. In addition, the measuring voltage can be varied over a wide range from 5 mV to 1 V rms. The principle of capacitance measurement function is based on vector-voltage-current ratio measurement method. The capacitance measuring range is 0.1 pF to 100 mF and that of the dielectric loss factor is 0.0001 to 19.999. Experiments were clone in the four probe configuration which eliminates errors due to residual impedance of test leads. The analyses has a built-in DC bias supply (providing a maximum ± 35 V DC voltage) which can be superimposed on the probing AC measuring field. Interfacing to a computer was established through the IEEE 488 bus. Thus all the functions could be controlled and monitored by the computer which also handled the data acquisition.

3.2.3 Static dielectric constant measurement

The block diagram of the experimental set-up used is shown in figure 3.5. Both the impedance analyses and the temperature reading digital multimeter (Keithley 181) were interfaced with a computer. At any desired frequency, tlie sample temperature was varied uniformly at a slow rate of $\sim 5^{o}K$/hour away from the transition and $\sim 2^{o}K$/hour close to it. The capacitance and temperature readings were continuously collected by the computer. For static measurements with a bias field, the required DC bias voltage was applied ancl the capacitance was measured at different temperatures.

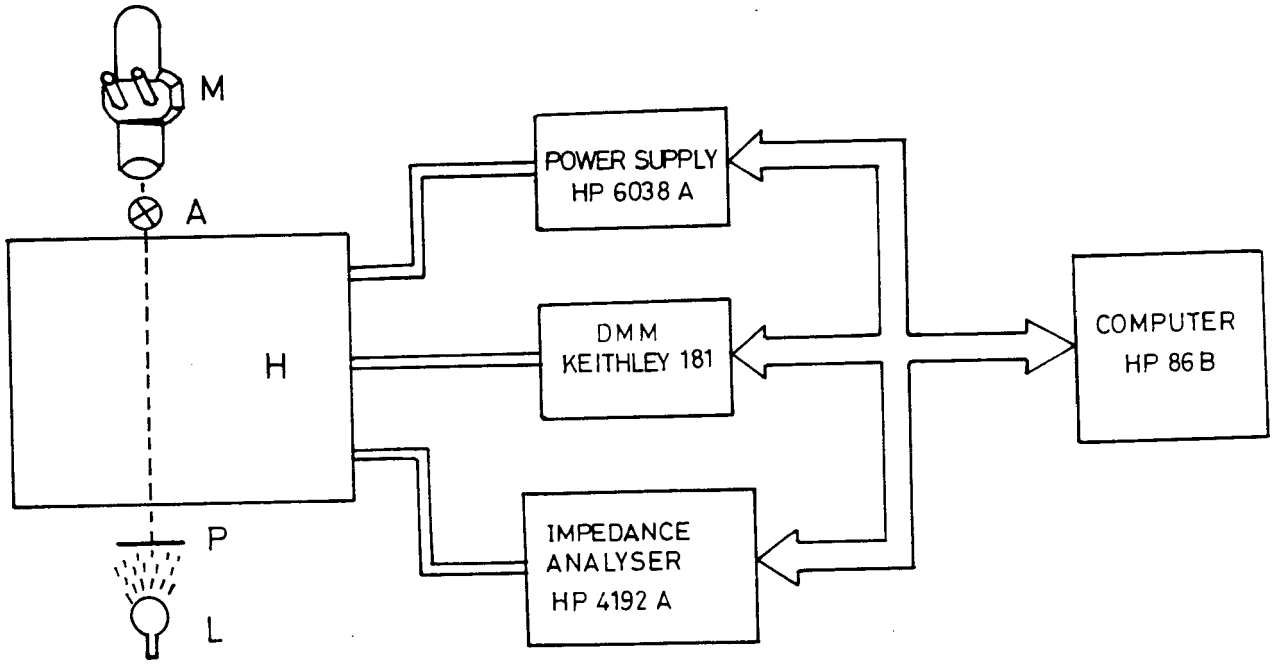

Fig.3.5. Block diagram of the dielectric measurement set-up.

H = Heating oven M = Microscope

P, A = Polarizer and Analyser

3.2.4 Dispersion measurements

The set-up used is the same as for static nieasurernents. For the frequency dependent dielectric constant measurements, the sample temperature was stabilized at the desired value and the microcomputer handled the frequency sweep by varying the frequency over the rarige of interest at a desired step value. The capacitance and the dissipation factor were measured as a function of the set frequency. Throughout the frequency sweep, tlie temperature was continuously monitored. The sweep measurements could also be carried out in the presence of a bias voltage.

The impedance analyser can he used up to a frequency of 13 MHz. But we have limited a11 our experiments to a maximum frequency of 600 KHz, as beyond this frequency the RC constant of the cell (due to the ITO layer) starts contributing to the measured dielectric values.

3.3 Results and Discussion

3.3.1 Static dielectric constant

Figure 3.6 is a plot of tlie temperature variation of $\epsilon_\perp$ measured at different frequencies for the compound C_{10} (see Table 3.1). As seen from the figure, in the *A* phase, $\epsilon_\perp$ does not, vary much with temperature. But, close to T_c, it increases drastically with decreasing temperature. The pretransitional increase in the value of $\epsilon_\perp$ (in the *A* phase) shows the existence of SM. In tlie C* phase tlie rapid increase in $\epsilon_\perp$, below T_c, confirms presence of GM. In the frequency range studied the behaviour on the C* side, i.e., GM, is strongly dependent on the frequency so much so that at 10 kHz $\epsilon_\perp$ value would be reduced to SM contribution only. One may observe similar effects with the application of a bias field and this is seen clearly in the figure 3.7. It

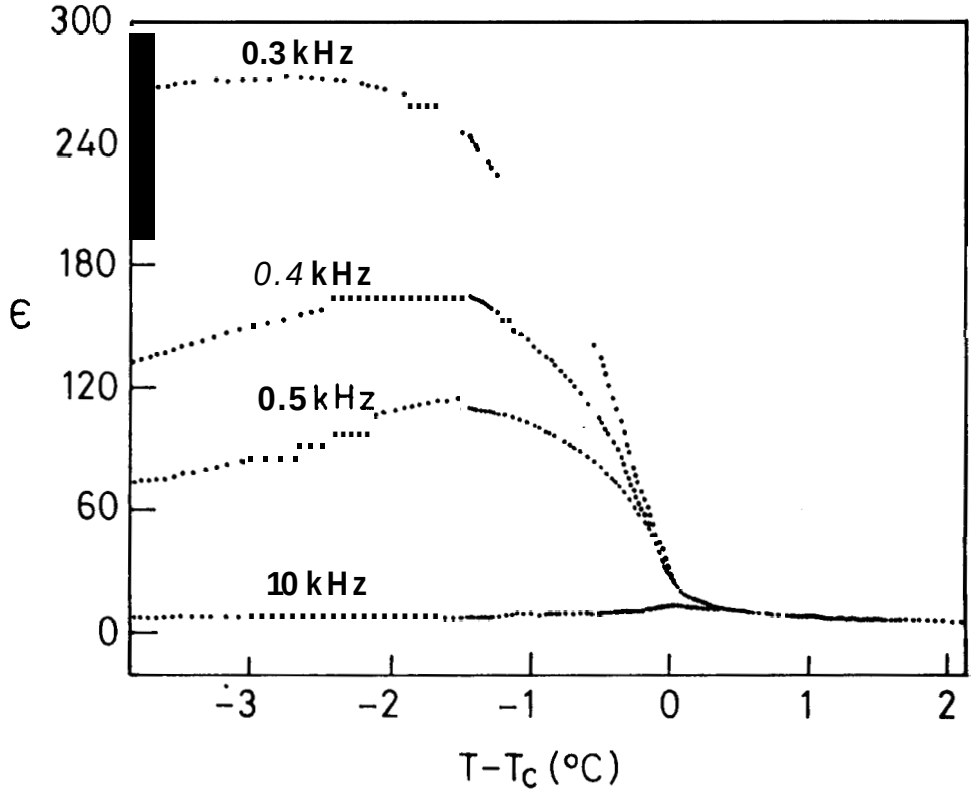

Fig.3.6. Influence of the frequency of measurement on the dielectric constant of compound C_{10}.

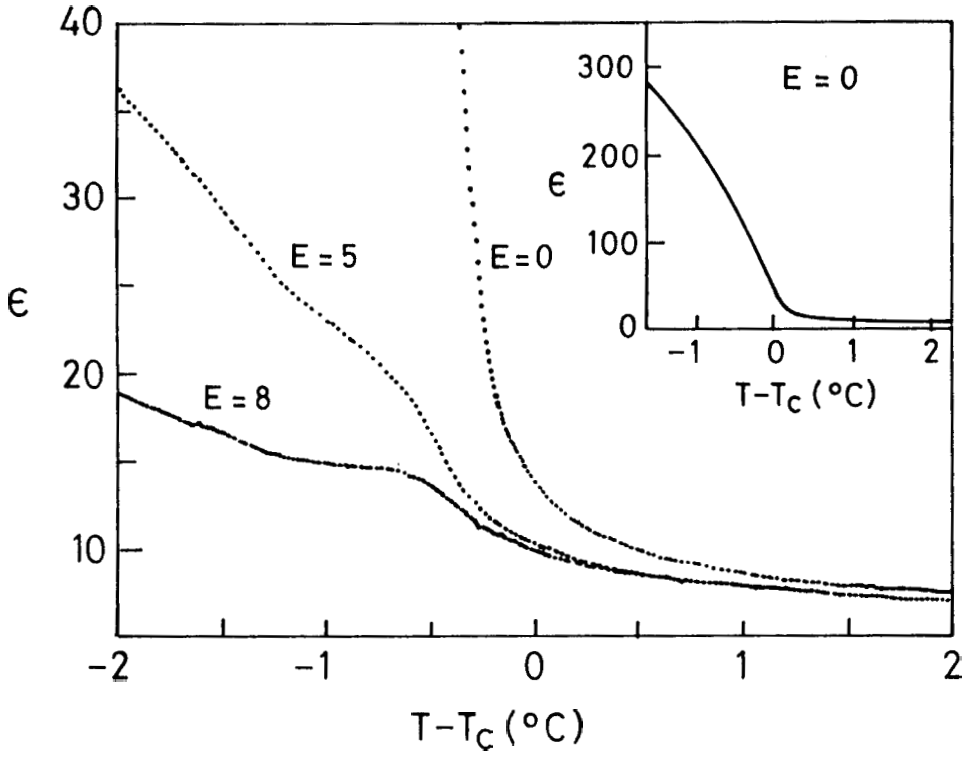

Fig.3.7. Effect of bias field on tlie static dielectric constant of compound C_{10}.

is evitlent from tliese figures that the effects observed as a function of frequency or DC bias voltage is caused by tlie GM relaxation. Another notable feature in tliese figures is that, there is a maximum in the dielectric constant at tlie transition when measured either at high frequency or with a high bias voltage implying that the contribution of SM reaches a maximum at T_c. To conclude, the thermal variation of dielectric constant measured at a few selected frequencies show the existence of SM and GM in a FLC. To have better understanding of these two director relaxation modes, we have carried detailed dispersion measurements on three compounds (listed in table 0.1) and the cffcct on both SM and GM caused by subtle molecular changes which, as seen in results of Chapter II, affects the magnitude of P_s. Thus these studies will also reveal, albeit in an indirect fashion, the effect of P_s on the behaviour of SM and GM.

3.3.2 Dispersion Studies

Before presenting the results let us recall tlie equations for the frequency dependence of the complex dielectric constant (ϵ^*). ϵ^* can be written in terms of its real (ϵ') and imaginary (ϵ'') components as'

$$\epsilon^*(f) = \epsilon' - j\epsilon'' = \epsilon_\infty + \frac{\Delta\epsilon}{1 + j\omega\tau} \tag{3.15}$$

Here $\Delta\epsilon(= \epsilon_0 - \epsilon_\infty)$ is the strength of the mode whose relaxation time is $\tau = \frac{1}{2\pi f_R}$ f_R being the relaxation frequency. ϵ_o and ϵ_∞ are the values of tlie dielectric constant at frequencies far below and far above f_R respectively. $\omega(= 2\pi f)$ is the measuring field frequency. A convenient method to determine tlie two characteristic parameters of the mode, $\Delta\epsilon$ and f_R, is to plot an Argand diagram of ϵ' vs. ϵ''. The plot (Fig. 3.8a) will be a seniicircle (corresponding to the positive values of ϵ''). Since eqn. **(3.15)** represents a Debye type relaxation, this semicircle is called a Debye semicircle, using

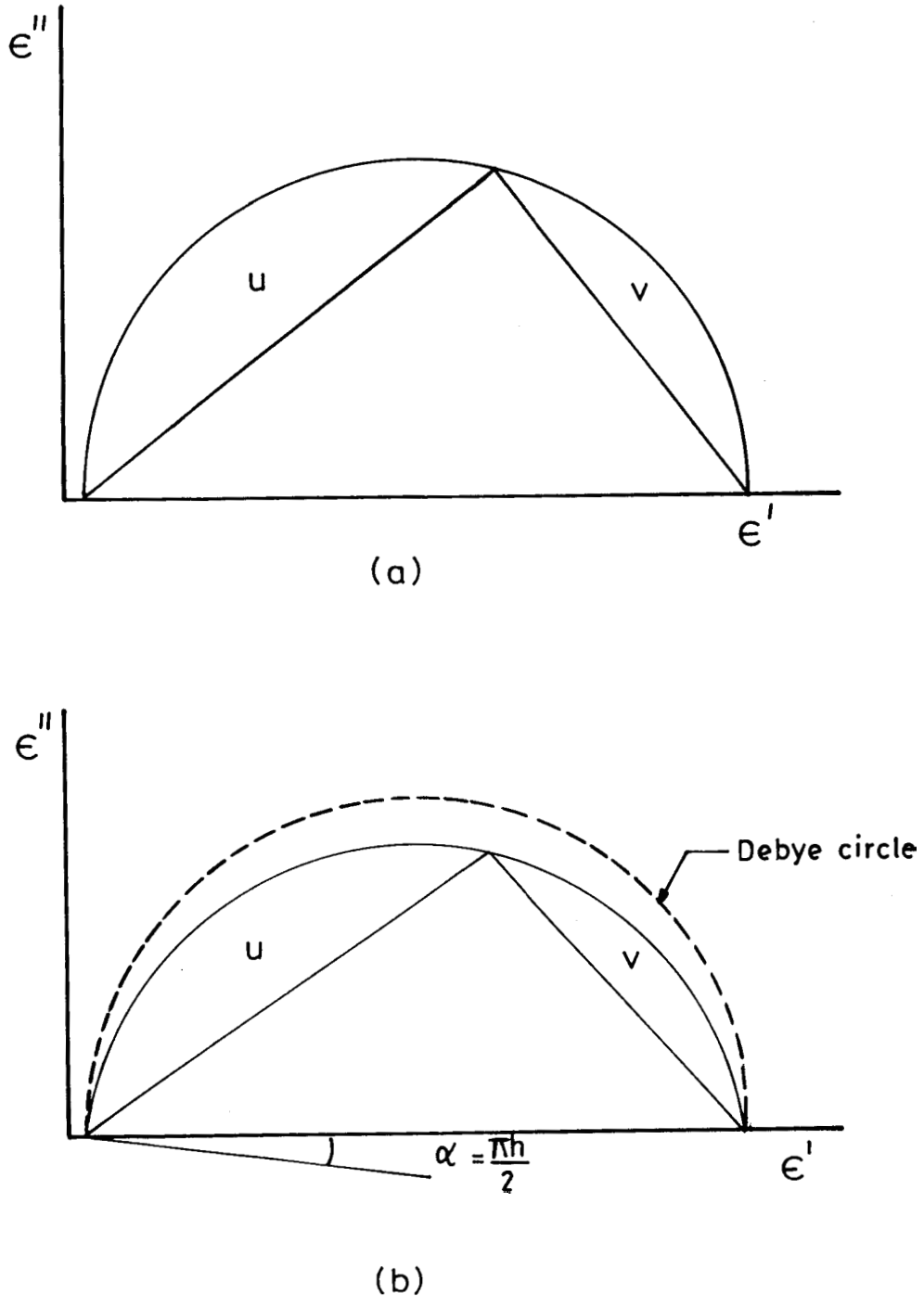

Fig.3.8. Plot of r' vs. ϵ" showing (a) a pure Debye type of relaxation, (b) a modified Debye, Cole-Cole, relaxation.

Table 3.1

Compounds used and their P_s values at T_c-T = 10 ° C

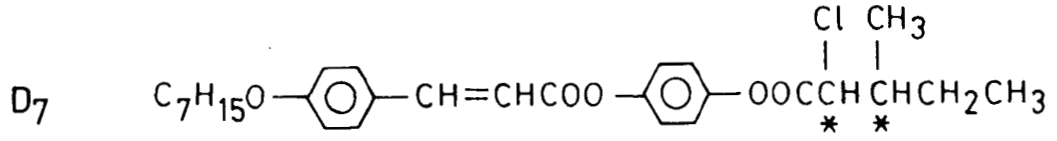

K 61.5 C* 68.5 A 88.0 CH 95.0 I $P_s = 1500\ \mu C/m^2$

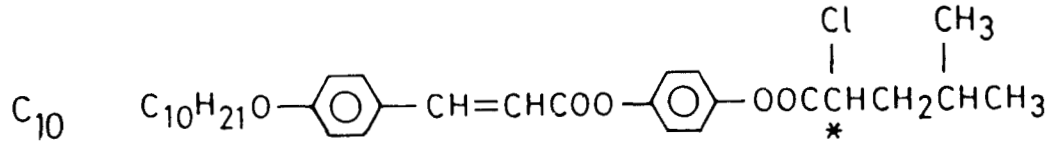

K 69.0 C* 78.0 A 92.5 I $P_s = 720\ \mu C/m^2$

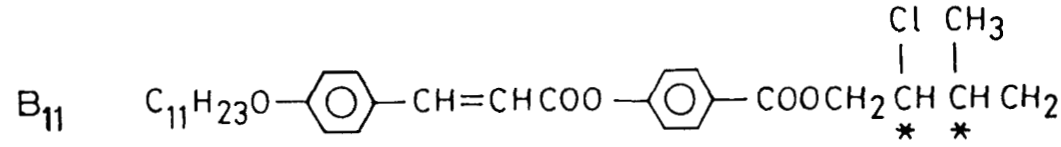

K 62.5 C* 68.5 A 88.0 I $P_s = 370\ \mu C/m^2$

which one can find $\Delta\epsilon = 2 \times \epsilon''_{max}$ and $f_R = f \times \frac{u}{v}$ with u and v defined as in figure 3.8a. However in the case of materials (like FLCs) which show a broader dispersion curve arid lower maximum loss than would be expected from Debye relation, tlie ϵ'' vs. ϵ' curve falls within the Debye semicircle (see Fig. 3.8b). For such cases Cole and Cole[17] suggested a modified form of tlie Debye equation

$$\epsilon^*(\omega) = \epsilon' - j\epsilon'' = \epsilon_\infty + \frac{\Delta\epsilon}{1 + (j\omega\tau)^{1-h}} \tag{3.16}$$

where h is a constant called the distribution parameter with $O \leq h < 1$. When h = 0 eqn. (3.16) reduces to a pure Debye type of relaxation. When h is non-zero, the centre of the Cole-Cole arc lies in the negative ϵ'' region, as shown in figure 3.8b. Rationalising eqn. (3.16), one gets,

$$\epsilon' = \epsilon_\infty + \frac{\Delta\epsilon[1 + (\omega\tau)^{1-h} \sin(\frac{\pi h}{2})]}{1 + (\omega\tau)^{2(1-h)} + 2(\omega\tau)^{1-h} \sin(\frac{\pi h}{2})} \tag{3.17}$$

$$\epsilon'' = \epsilon_\infty + \frac{\Delta\epsilon(\omega\tau)^{1-h} \cos(\frac{\pi h}{2})}{1 + (\omega\tau)^{2(1-h)} + 2(\omega\tau)^{1-h} \sin(\frac{\pi h}{2})} \tag{3.18}$$

Equation (3.17) or (3.18) can be used to determine the values of $\Delta\epsilon$ and f_R. Except near tlie transition in tlie C* phase, eqn. (3.17) or (3.18) is sufficient to describe the relaxation behaviour. However, close to tlie transition, both GM and SM contribute to the dielectric constant. In such cases, it has been shown[27] that ϵ^* can be written as a linear combination of the two modes involved.

$$\epsilon^*(f) = \epsilon' - j\epsilon'' = \epsilon_\infty + \frac{\Delta\epsilon_G}{1 + (j\omega\tau_G)^{1-h_G}} + \frac{\Delta\epsilon_s}{1 + (j\omega\tau_s)^{1-h_s}} \tag{3.19}$$

where $\Delta\epsilon_i$ (i = SM and GM) represents the strength, τ_i the relaxation time and h_i the distribution parameters of the modes. Rationalisation of eqn. (3.19) leads to equations similar to equations 3.17 arid 3.18.

We have fitted our experimental data of (ϵ^*(f),f) in the *A* phase and C* phase (far below T_c) to eqn. (3.17), to obtain the dielectric strength, relaxation frequency

of SM and Ghl relaxations respectively and (ϵ_∞). The (ϵ^*(f), f) data in the C* phase close to T_c has been fitted to a rationalised expression of eqn. (3.19) to separate out tlic relaxation parameter of the two modes. The fitting has been carried out using a non-linear "least squares" program based on the Marquardt algorithm by floating all tlic parameters involved. In all the cases tlic distribution parameter h_i was found to be quite small (≈ 0.1).

Figures 3.9a-c show representative Cole-Cole diagrams obtained for the compound C_{10}; figures 3.9a in tlie A phase, 3.9b in the C* phase close to T_c and 3.9c in the C* phase away from T_c. The solid line in tlie figures is tlie fit to eqn. (3.18). Plots in figures 3.9a and 3.9c exhibit single relaxation behaviour due to SM arid GM respectively. When the temperature is close to T_c in tlie C* phase, tlie Cole-Cole plot (Fig.3.9b) shows tlie simultaneous existence of both the relaxations (tlie solid line is fit to eqn. (3.19)). Normally it is difficult to, except very close to tlie transition, separate out the two modes. This is because, as seen from the figure, the strength of SM is much smaller compared to that of GM. Also the strength of the SM decreases rapidly as T_c – T is increased. However, owing to the large value of P_s in D_7 we have been able to resolve the two over a temperature range of 0.8^oC in the C* phase, which is a larger temperature range (in the absence of the bias field) than in any other previous report.[17] For tlic same reason the SM could he studied up to 3^oC in the A phase. In fact this point is quite clear when we note that for the three compounds these ranges are 0.8°; 3.0" for D_7, 0.5'; 1.5^o for C_{10} and 0.07; 0.5^oC for B_{11} respectively.

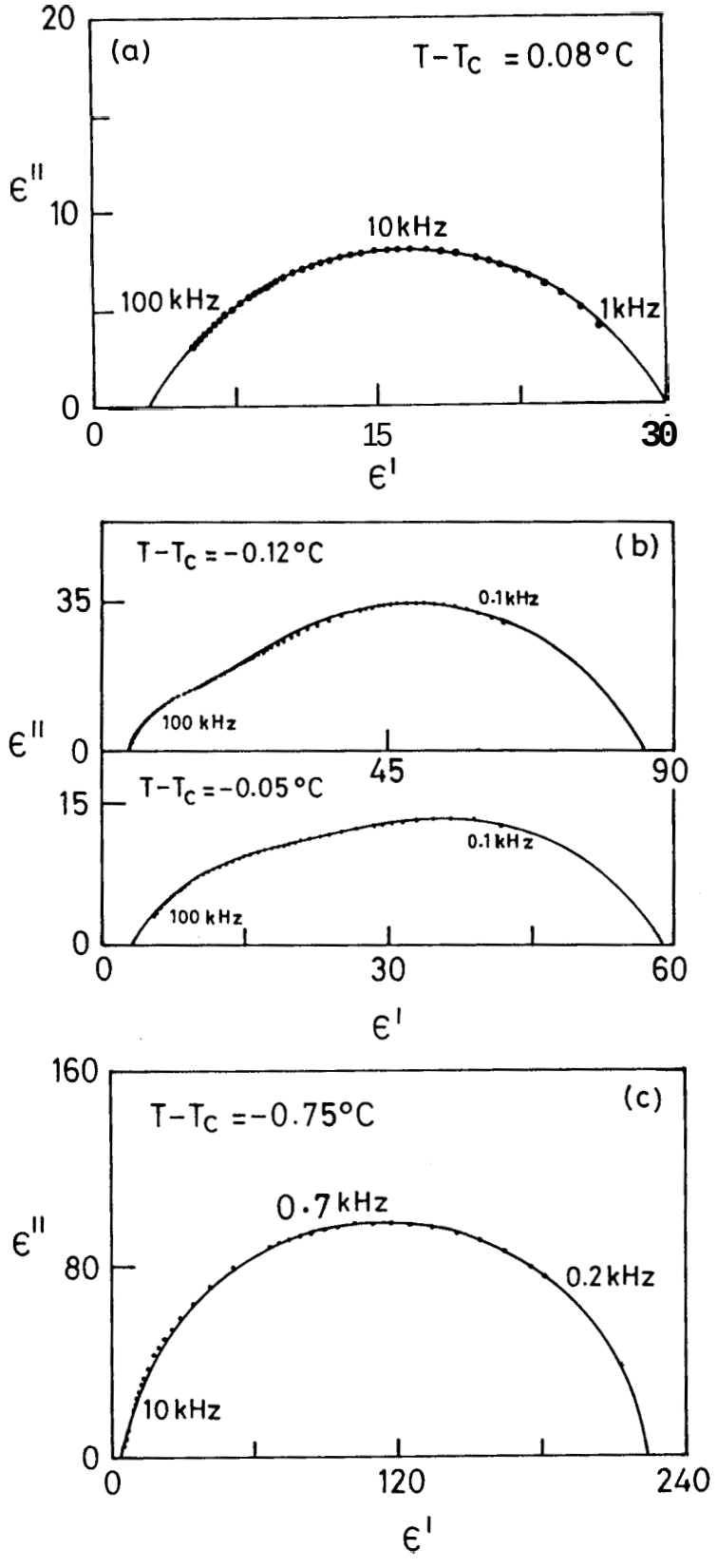

Fig.3.9. Representative Cole-Cole diagrams for compound C_{10} in (a) A phase; (b) C* phase near T_c; (c) C* phase away from T_c. Notice the double Cole-Cole behaviour in (b).

3.3.3 Soft mode relaxation

Figures 3.10-3.12 are tlie plots of inverse soft mode strength $1/\Delta\epsilon_s$ and relaxation frequency f_s for tlie three compounds. The salient features observed in the figures are (1) In tlie *A* phase f_s varies linearly with temperature while $1/\Delta\epsilon_s$ is non linear. 2) In tlie C* phase botli f_s and $1/\Delta\epsilon_s$ are linear with temperature. Most of the earlier experiments have also shown tlie linear behaviour of f_s, but only a few observations of non linear variation of $1/\Delta\epsilon_s$ exist. 3)At T_c botli f, and $1/\Delta\epsilon_s$ reach a lion-zero minimum (i.e., the SM strength has a finite maximum). The minima being non-zero is as cxpectcd for improper ferroelectrics. f_o, the value of f_s at T_c is different for compounds D_7, C_{10} and B_{11} – $f_o(D_7) > f_o(C_{10}) > f_o(B_{11})$ - and appears to depend on tlie magnitude of P,. In tlie following we shall attempt to explain tlie beliaviour of botli f_s and $1/\Delta\epsilon_s$ with the help of equations 3.8-3.11 given by tlie generalised mean field model. According to eqn.(3.9) f_s has a linear temperature dependence if the ratio of $\frac{(K_3 - \epsilon\mu^2)q_o^2}{2\pi\eta_s}$ is independent or weakly dependent on temperature.[35] The non-linear thermal variation of $1/\Delta\epsilon_s$ may be due to tlie temperature dependence of tlie elastic torque $(K_3 - \epsilon\mu^2)q_o^2$ and bilinear coefficient C (see eqn.(3.8)). However it may be recalled that the coefficient C is shown to be independent of temperature for low as well as high P_s materials.[36] Thus one reason for the 11011-linearbehaviour of $1/\Delta\epsilon_s$ could he that the twist to piezo energy ratio $\frac{(K_3 - \epsilon\mu^2)q_o^2}{\epsilon^2 C^2}$ may be changing with temperature (we see later that this is true in the C* phase). Due to these reasons the product $\Delta\epsilon_s$ x f_s should also be non-linear close to T_c. This is indeed the case as seen from the plots (figures 3.13-3.15) of $\Delta\epsilon_s f_s$ vs. $T - T_c$ for tlie three compounds. Following Gouda *et al.*,[37] we have tried to describe this behaviour of $\Delta\epsilon_s f_s$ in the *A* phase with a power law of the type $\Delta\epsilon_s f_s \propto (T - T_c)^\beta$. The values of β for the three compounds are 0.45, 0.37 and 0.2 respectively for D_7, C_{10} and B_{11}.

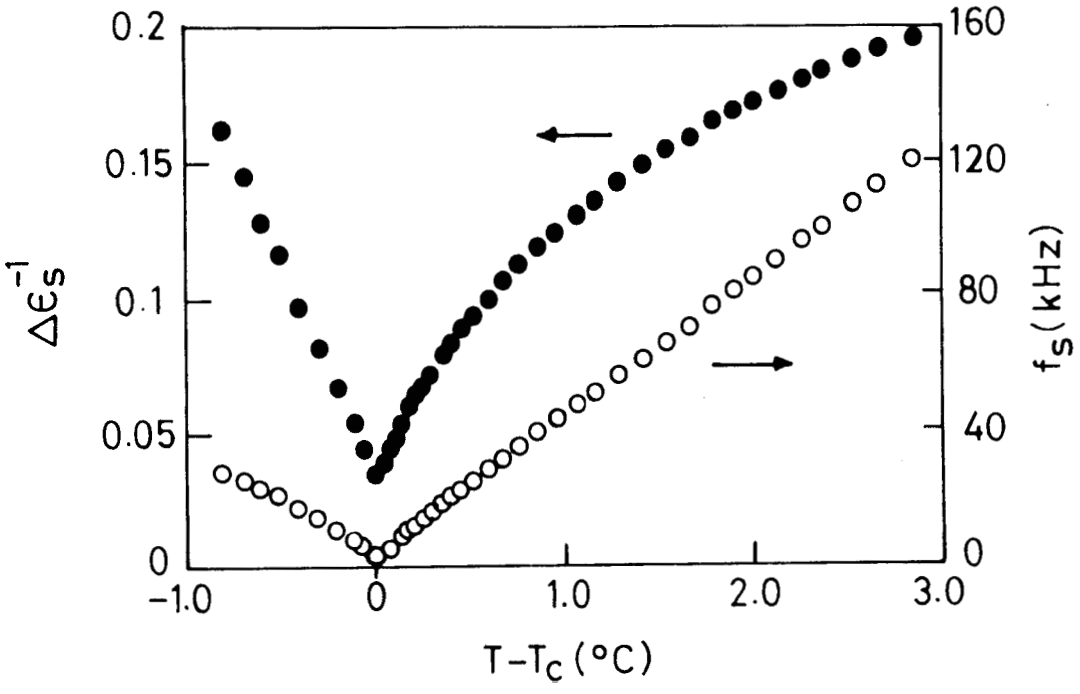

Fig.3.10 Temperature dependence of soft mode relaxation frequency (f_s) arid inverse dielectric strength ($1/\Delta\epsilon_s$) for compound &.

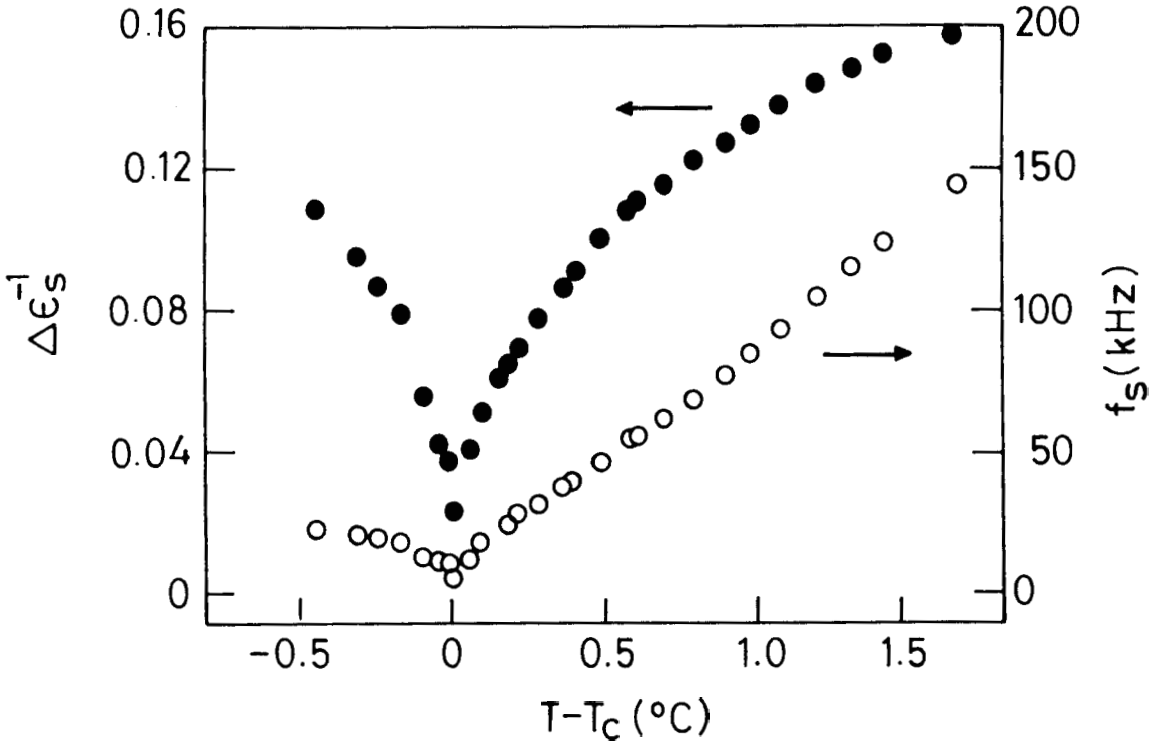

Fig.3.11. Thermal variation of f_s and $1/\Delta\epsilon_s$ for compound C_{10}.

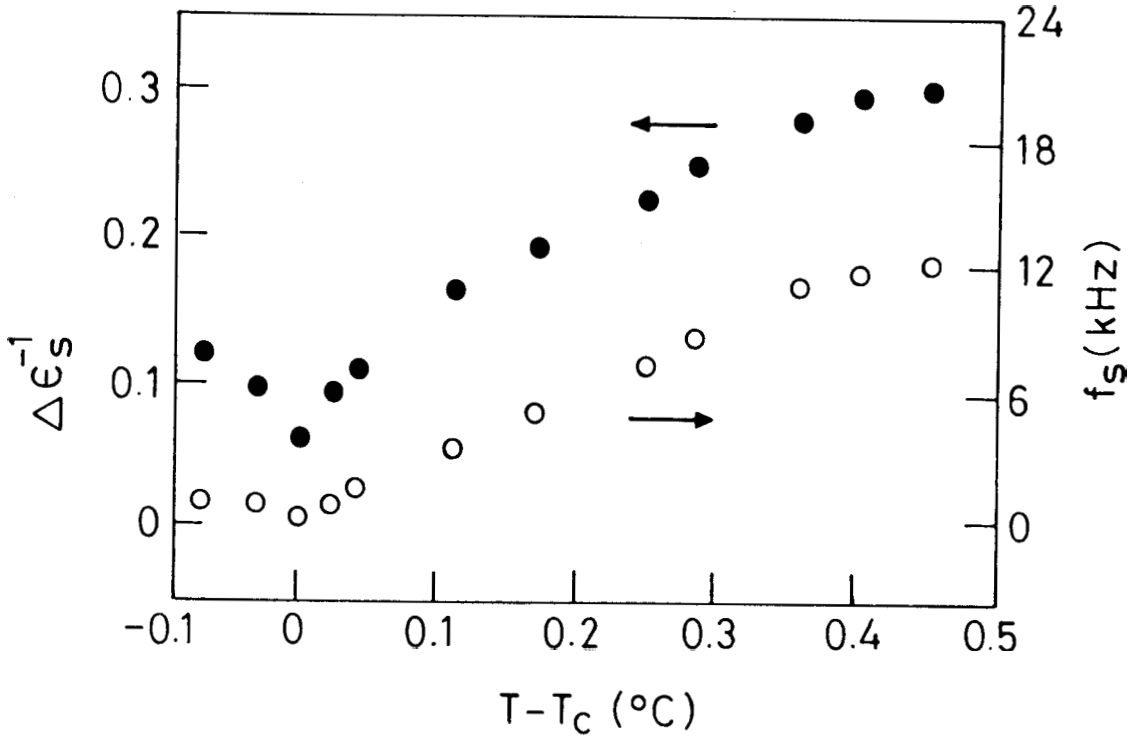

Fig.3.12. Thermal variation of f_s and $1/\Delta\epsilon_s$ for compound B_{11}.

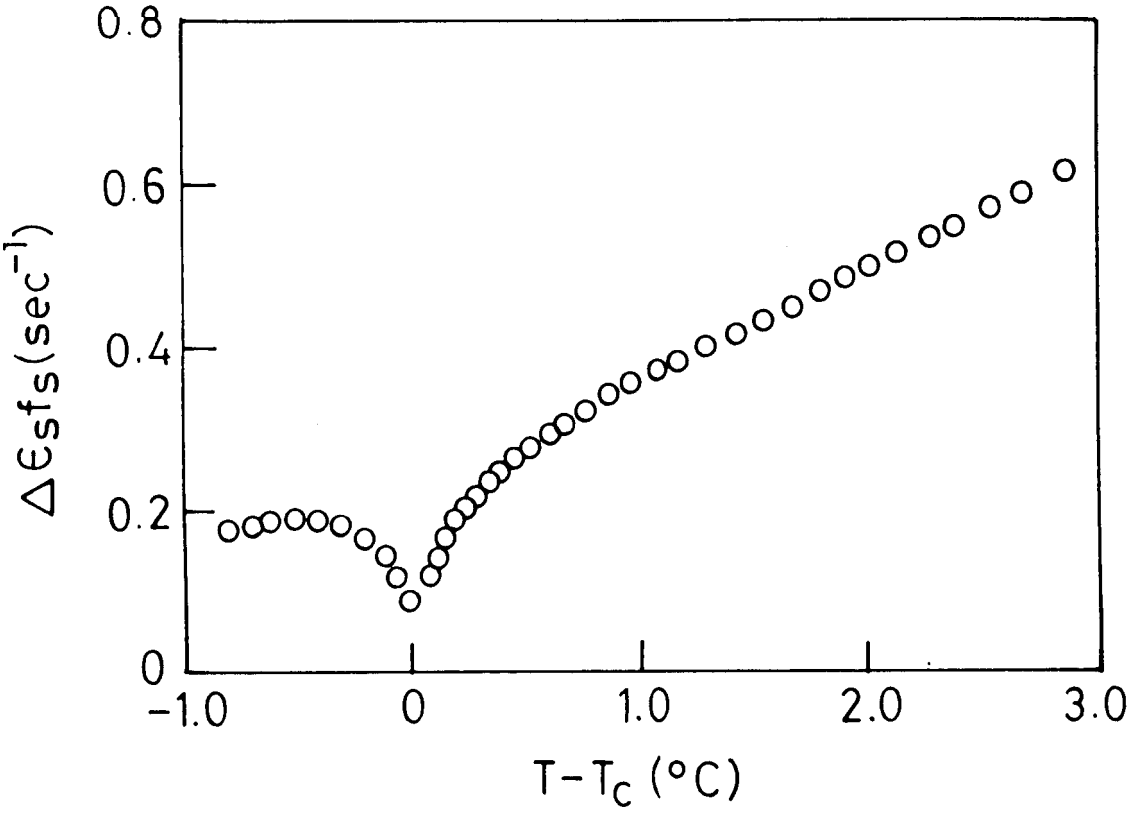

Fig.3.13. Plot of the product $\Delta\epsilon_s f_s$ vs. temperature for compound D7.

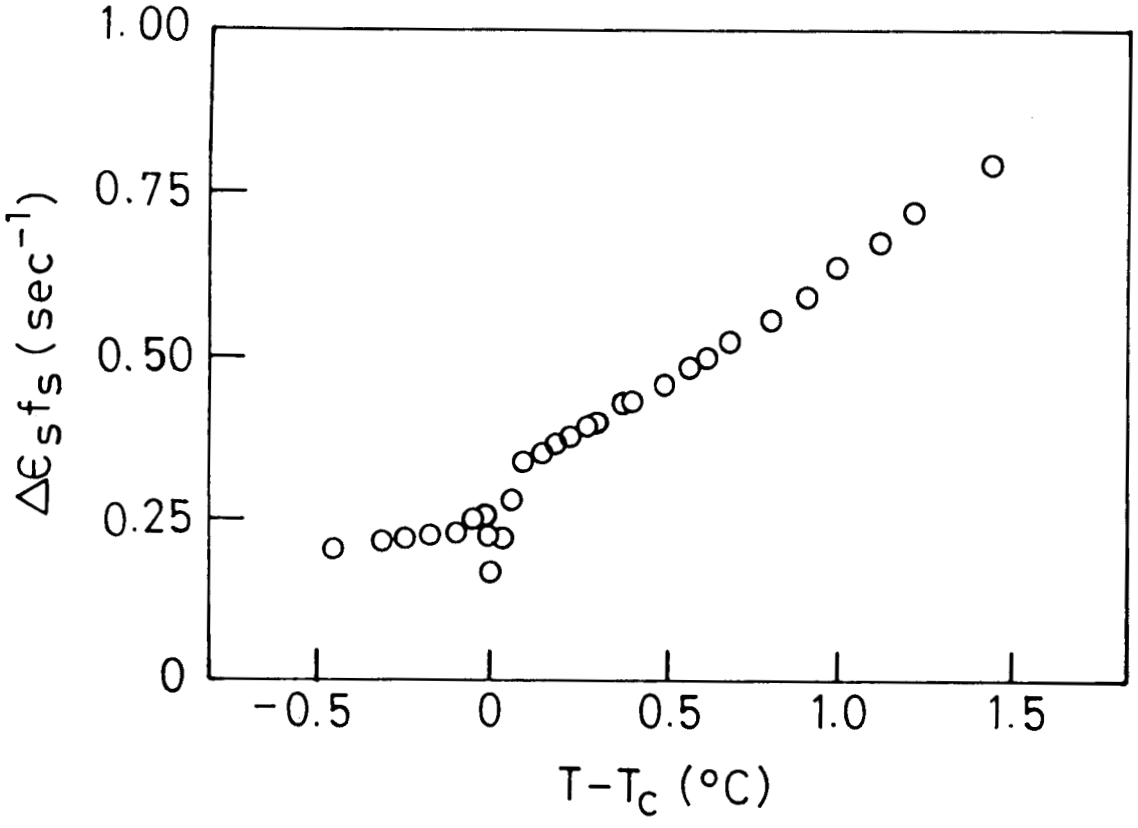

Fig.3.14. Temperature dependence of $\Delta\epsilon_s f_s$ for compound C_{10}.

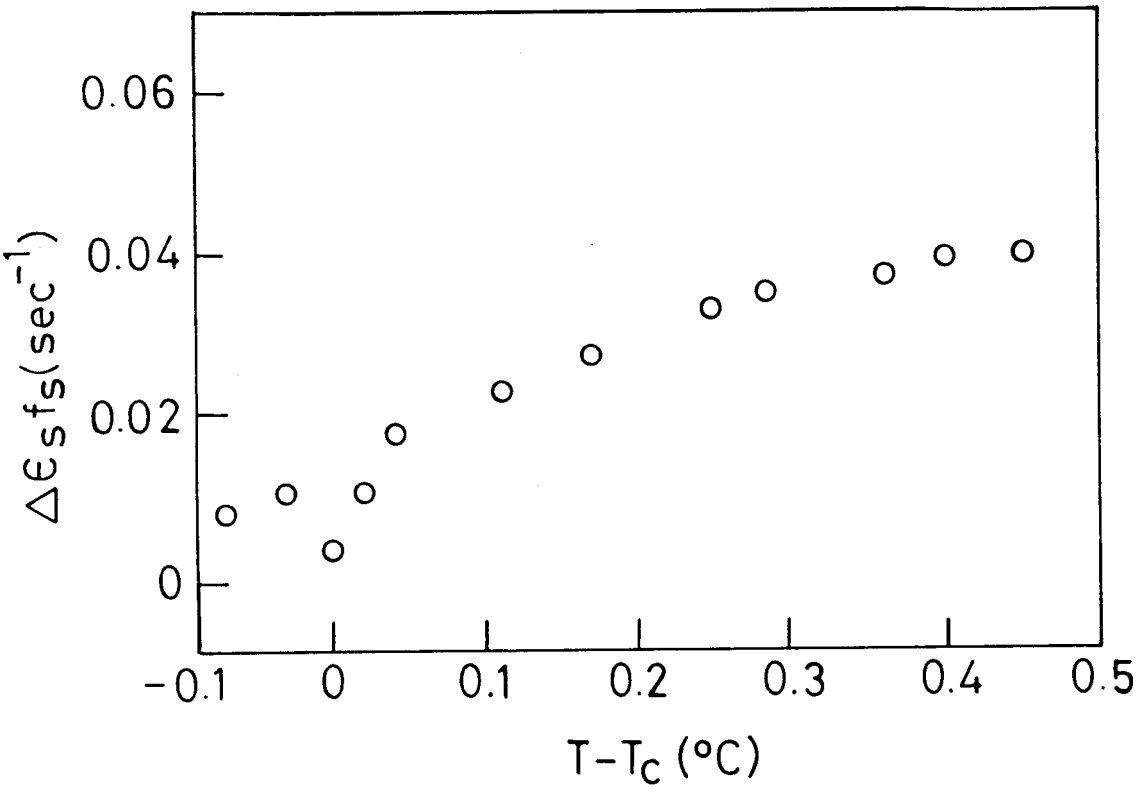

Fig.3.15. Plot of $\Delta\epsilon_s f_s$ vs. temperature for compound B_{11}.

3.3.4 Goldstone mode relaxation

The thermal variation of $\Delta\epsilon_G$ and f_G for the three compounds are shown in figures 3.16-3.18. Some notable features arc -

1. f_G is observed to be weakly dependent on temperature away from the transition, but varies strongly very close to T_c.

2. The minimum of f_G is not at T_c but slightly below it.

3. The actual value of f_G seems to be directly related with the magnitude of P_s, i.e., $f_G(D_7) > f_G(C_{10}) > f_G(B_{11})$.

4. $\Delta\epsilon_G$ is zero at T_c arid increases rapidly in tlie C^* phase. For C_{10} it appears to stabilise away from T_c. Whereas D_7 and B_{11} show variation of $\Delta\epsilon_G$ even away from T_c.

According to Legrand and Parneix[38] the relative twist to piezo energy ratio parameter $\mathbf{Q^2}$ is defined as $\mathbf{Q^2} = \frac{Kq^2}{\chi_\infty c^2}$, where K is the renormalized twist elastic constant and $\chi_\infty = \frac{1}{4\pi}(\epsilon_\infty - 1)$. These authors give a more practical definition for $\mathbf{Q^2}$ as $Q^2 = \frac{2\pi\chi_\infty}{\Delta\epsilon_G}$. Using this relation we have calculated $\mathbf{Q^2}$ for the compound C_{10} at two different temperatures. The values are 0.004 at $T_c - T$ = 6°C arid 0.09 at. T_c – T = 0.02°C. These numbers may be compared with the value of Q^2 = 0.2 for DOBAMBC[10] ($P_s \approx 30\mu C/m^2$) and Q^2 = 0.003 for a material[38] with $P_s = 500\mu C/m^2$ away from T_c. This appears to suggest that tlie value of $\mathbf{Q^2}$ is inversely proportional to P_s. Also tlie values of Q^2 calculated show that $\mathbf{Q^2}$ varies substantially with temperature.

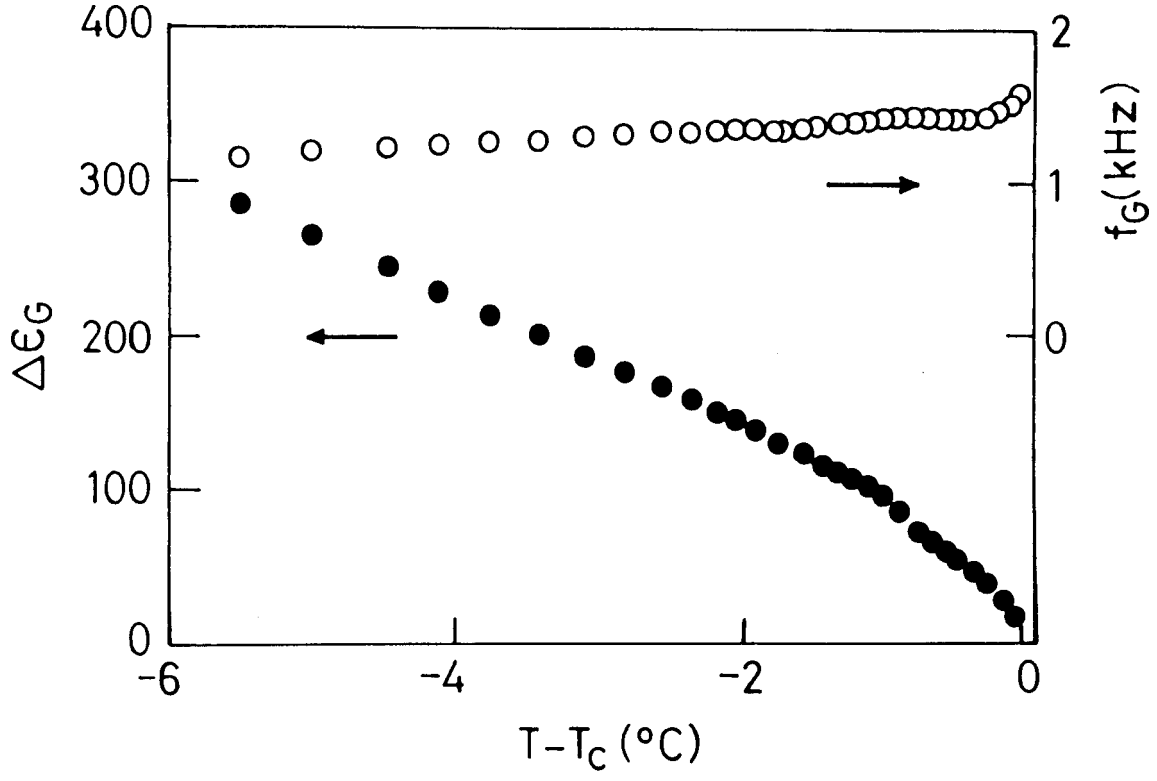

Fig.3.16. Temperature dependence of Goldstone mode frequency (f_G) arid dielectric strength ($\Delta\epsilon_G$) for D_7

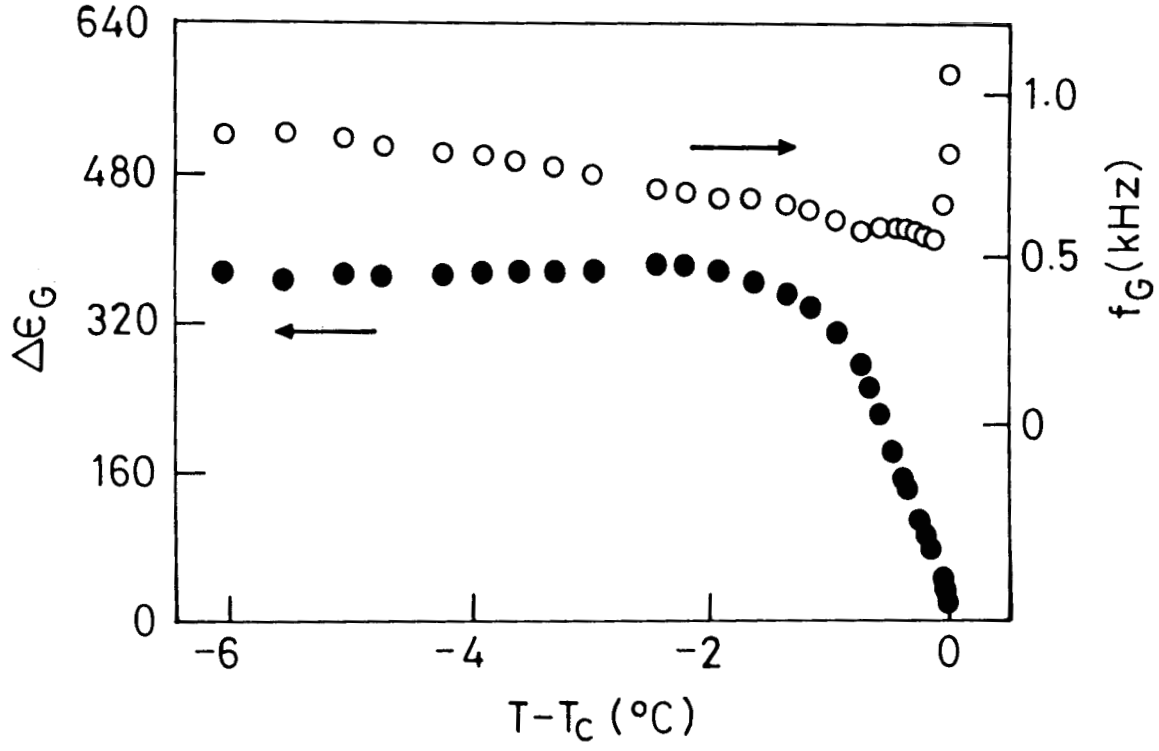

Fig.3.17. Thermal variation of f_G and $\Delta\epsilon_G$ for compound C_{10}.

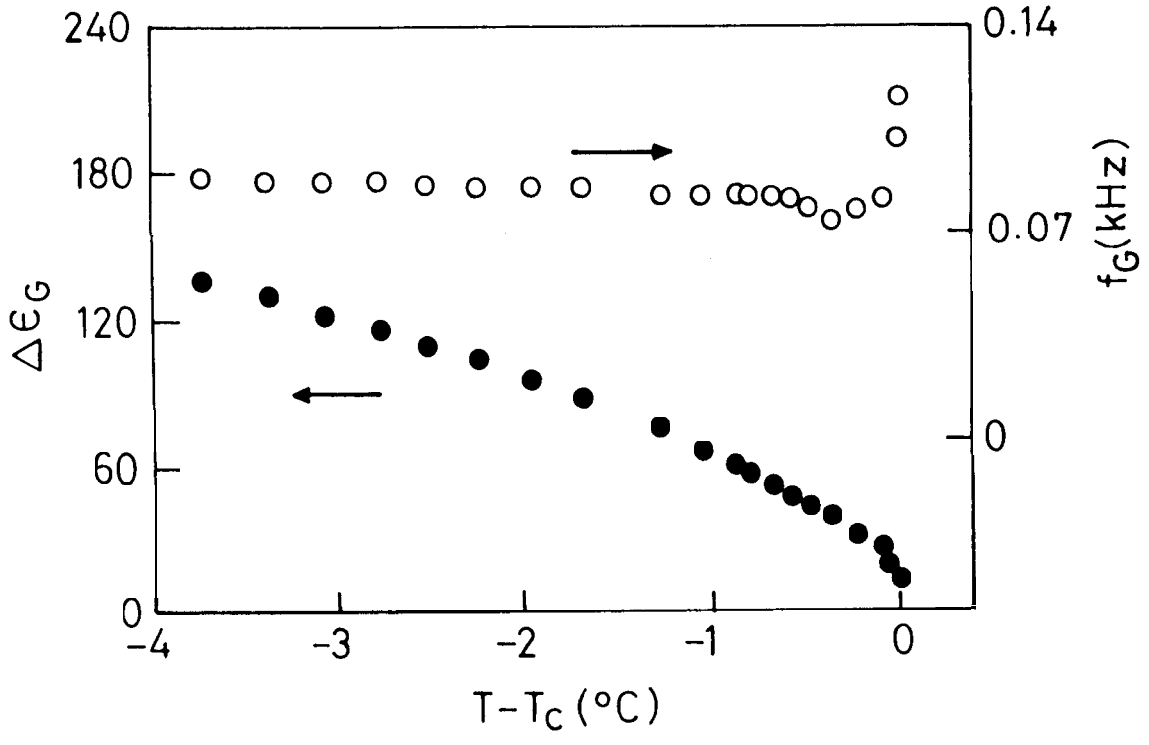

Fig.3.18. Thermal variation of f_G and $\Delta\epsilon_G$ for compound B_{11}.

3.3.5 Effect of bias field on the soft mode

As mentioned earlier the main problem in studying the SM in the C* phase is that tlie dielectric strength of the Ghl drowns that due to the Shl even slightly away from T_c. One well known technique[18,19,39] to overcome this problem is to apply a DC bias field high enough to unwind the helical structure. We have used this method to study the SM relaxation in one material, viz., C_{10}. Figures 3.19 and 3.20 are the plots of $1/\Delta\epsilon_s$ and f_s as a function of temperature obtained using a bias voltage of 20 kV/cm; for the sake of coinparison the zero bias values are also plotted. While zero bias data show sharp minima at the transition, tlie minimum is broad in the presence of a bias voltage. Also, the values of $\Delta\epsilon_s$ arid f_s at the transition are different in the two cases: $(\Delta\epsilon_s)_{E=0} = 43.5$ and $(\Delta\epsilon_s)_{E=20} = 5.8$ and $(f_s)_{E=0} = 3.8$ kHz and $(f_s)_{E=20} = 53.7$ kHz. Here E denotes the bias field applied. The higher f_s value in the presence of bias field may he due to the reason that the high bias field rigidly holds the dipoles (molecules) in the direction of the field and this additional rigidity increases tlie value of f_s. For the same reason At, for the bias case is smaller than that for zero bias.

3.3.6 Effectofchainlengthonthedielectricproperties

The length of the alkyl chain plays a crucial role in liquid crystals. In general this parameter affects the transition temperatures and stability of different mesophases. In FLCs, tlie alkyl chain length alters, as seen in Chapter II, the magnitude and nature of thermal variation of P_s. Results presented in Chapter IV also show that even the rotational viscosity γ_ϕ is influenced by this. Thus, it would he interesting to study the correlation between this parameter and the behaviour of GM and SM.

For this purpose dielectric measurements were carried out on three homologues n

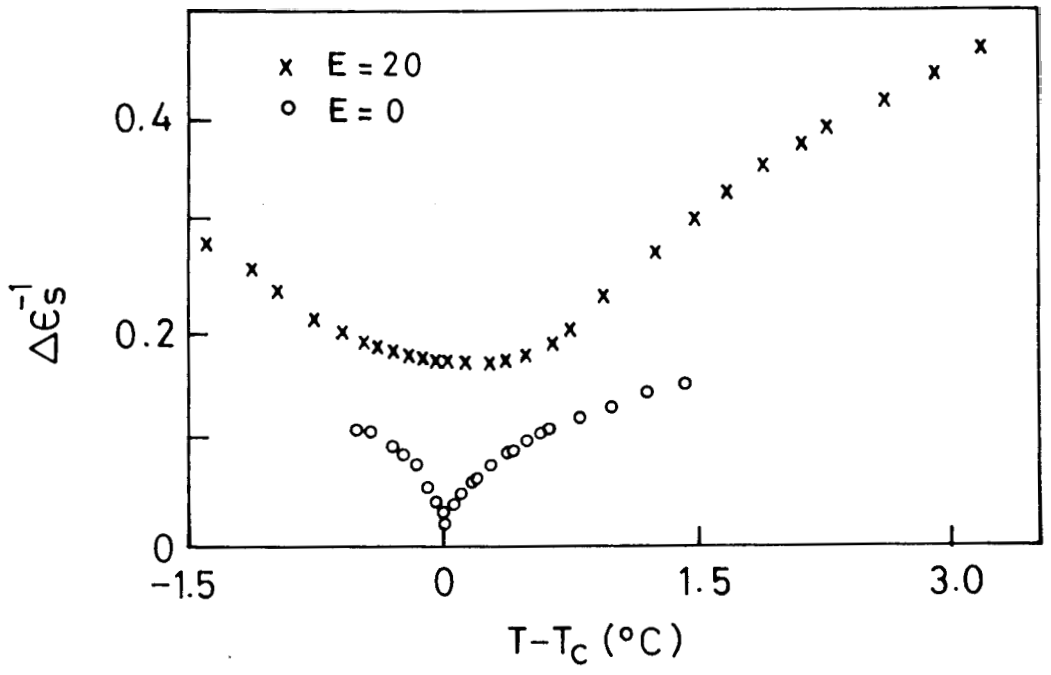

Fig.3.19. Plot of $1/\Delta\epsilon_s$ vs. temperature with no bias (○) and 20 kV/cm bias field (x) for compound C_{10}.

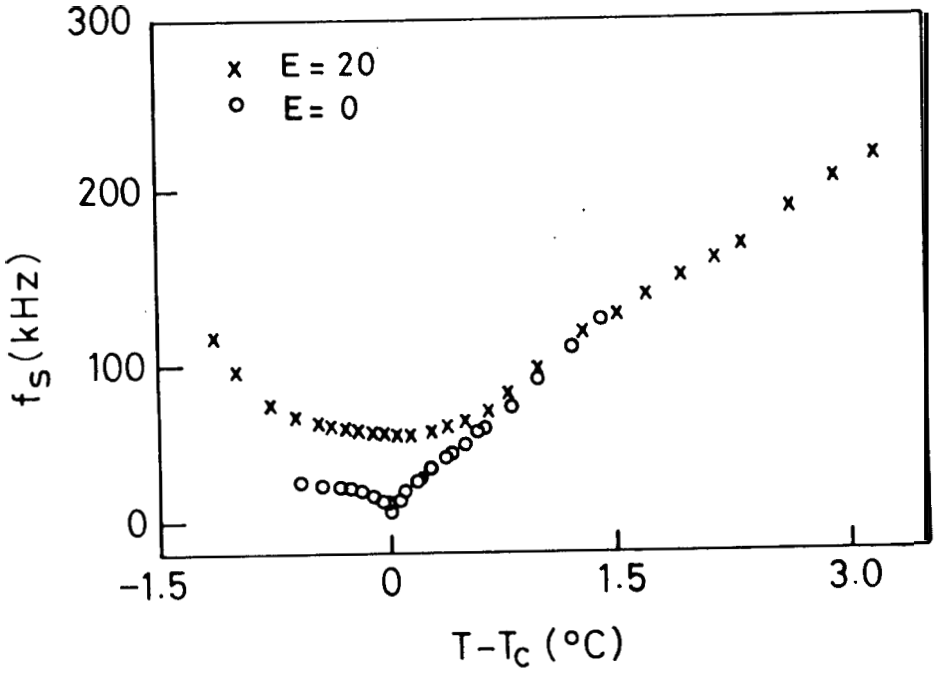

Fig.3.20. Plot of f_s vs. temperature with no bias (○) and **20** kV/cm **bias** field (x) for compound C_{10}.

= 6 to 8 of tlie series [S]-4′-(2-chloro-4-methyl pentanoyloxy)phenyl *trans*-4″-n-alkoxy cinnamates (C, series, n = 6-8). The transition temperatures and the molecular structure of the compounds is already given in Table 2.3.

Plots of tlie thermal variation of $\Delta\epsilon_G$ and f_G for the three compounds are shown in figures 3.21 and 3.22. The salient features seen arc -

1. The value of $\Delta\epsilon_G$ increases with increasing chain length, but not strictly proportional to it, for e.g., tlie difference in $\Delta\epsilon_G$ between C_7 and C_8 is larger than that between C_6 and C_7.

2. The trend in f_G (figure 3.22) is different. f_G for C_7 is much greater than those for C_6 and C_8 so much so that a sort of *odd-even* effect is observed. The product $\Delta\epsilon_G f_G$ also shows tliis type of behaviour. One reason for tliis could be tlie odd-even behaviour in tlic pitch.[40] But that were to be tlic sole factor it should have been manifested in tlie $\Delta\epsilon_G$ behaviour also; but figure 3.21 does not support this idea. In fact, this possibility can he ruled out as the product $\Delta\epsilon_G f_G$ which is independent of pitch also shows the odd-even effect. We notice from eqn.(3.13) that $f_G = \frac{K_3 q^2}{2\pi\gamma_G}$. Thus the odd-even nature in f_G may be due to the alternation in tlie value of the ratio $\frac{K_3 q^2}{\gamma_G}$ with chain length. To verify this we have calculated the value of $K_3 q^2$ by using tlie expression for $\Delta\epsilon_G$ (details are given in next section) and obtained tlie value of γ_G from the Diamant method[41] (described in the next chapter). The calculated values of the ratio $\frac{K_3 q^2}{\gamma_G}$ at $T_c - T = 5^oC$ for the three compounds are: 2470 (for C_6), 3170 (for C_7) and 2850 (for C_8), i.e., non-monotonic with chain length. Hence this must be the reason for the alternation in the value of f_G for the three homologues. The ratio of the quantities $(P/\theta)^2$ and γ_G also shows such an alternation and accounts for the odd-even behaviour seen in $\Delta\epsilon_G f_G$.

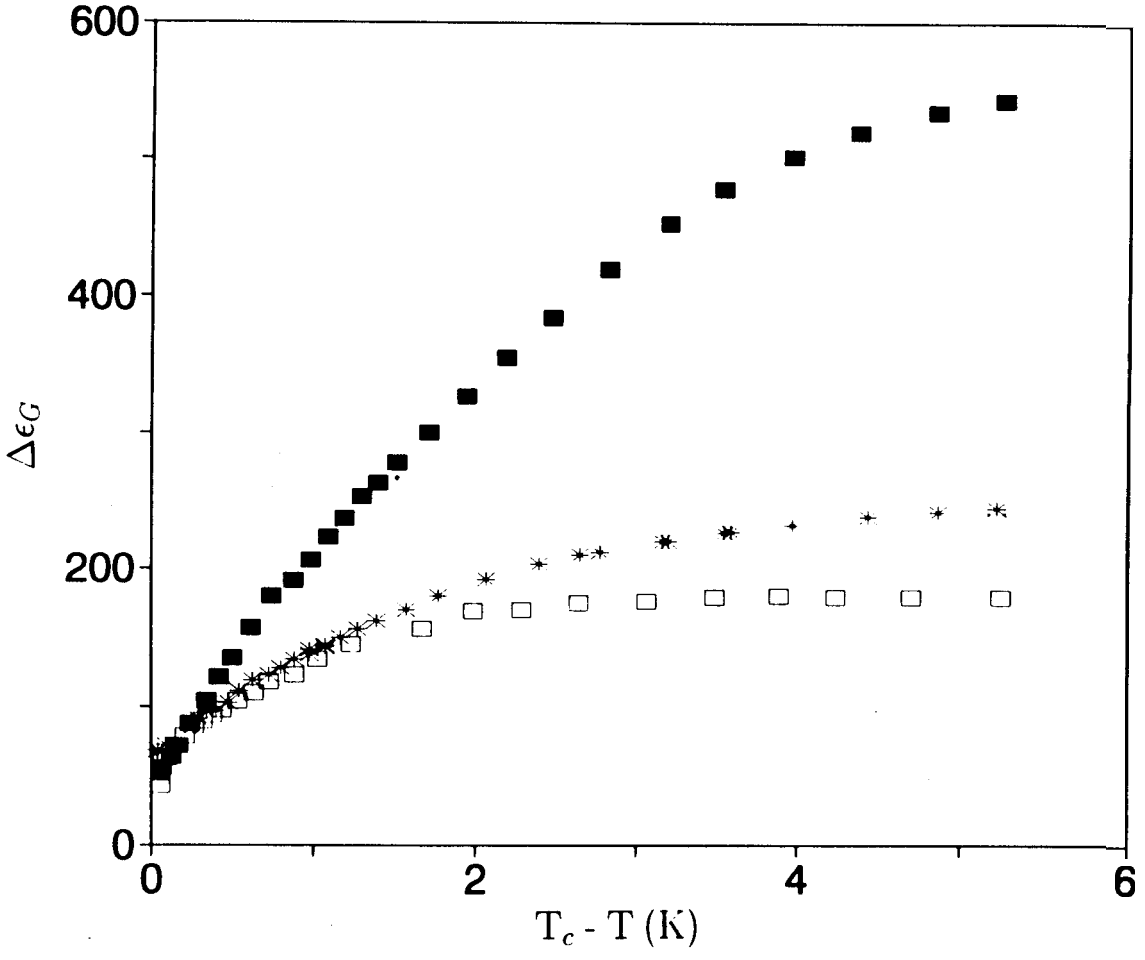

Fig.3.21. Effectof chain length on the temperature dependence of $\Delta\epsilon_G$ for C_6 (□), C_7 (*) and C_8 (■).

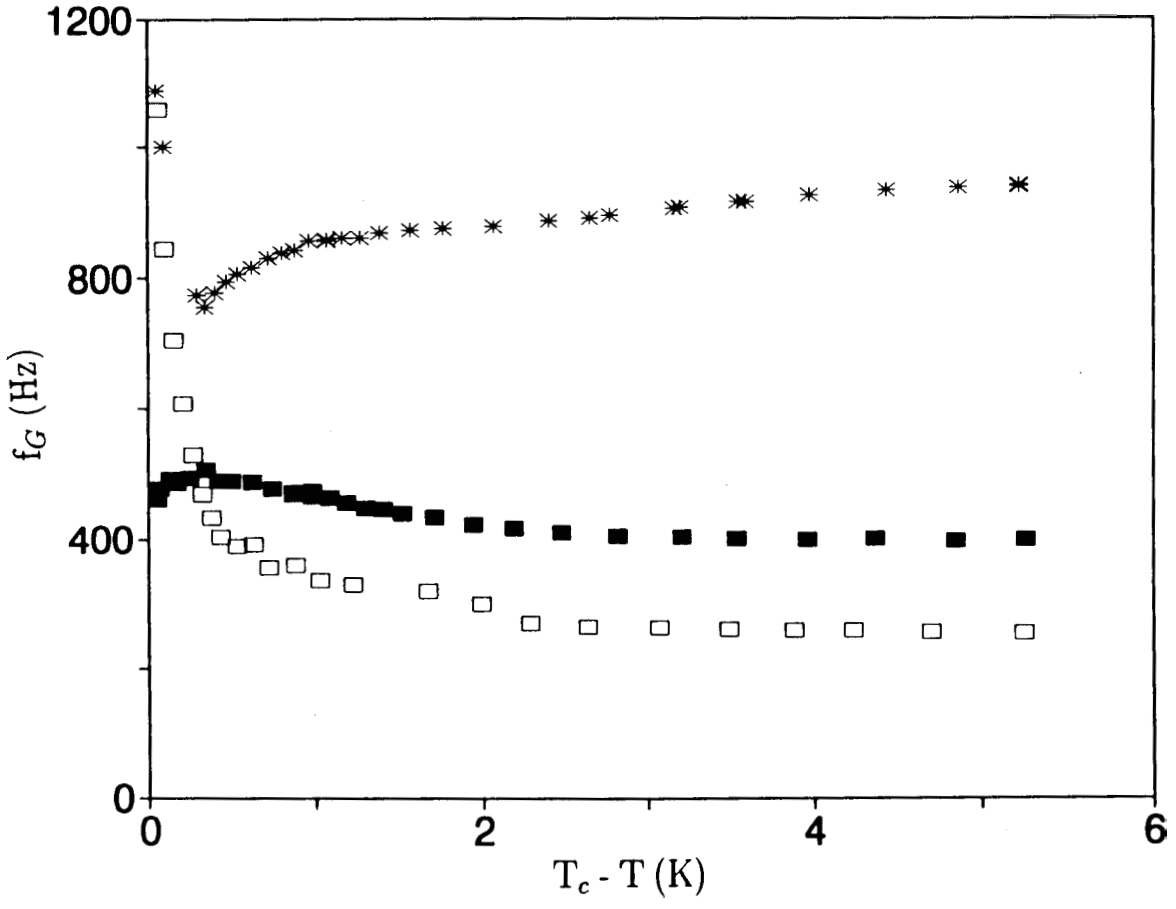

Fig.3.22. Effect of chain length on the thermal variation of f_G for C_6 (□), C_7 (*) and C_8 (■).

While looking at, the predictions of the generalised mean field theory,[32] we find a remarkable similarity between tlie experimental data of figures 3.21 and 3.22 and the theoretical curves obtained for different values of β (see figures 3.4a and 3.4b); here β is the effective $\mathrm{P}-\theta$ coupling constant defined in the earlier section. In particular, as the chain length is varied, drastic changes in the magnitude of $\Delta\epsilon_G$ and f_G, presence or absence of a pronounced minimum in f_G, etc., arc seen. Thus for the compounds $C_6 - C_8$ one should expect the β values to change significantly with increase in chain length. We have determined the β values by fitting the data of P_s (obtained by Diamant method) and θ (obtained by X-ray diffraction method) to eqn. (3.14). The parameters P^*, θ^* and β obtained for the three cornpounds are listed in the Table 3.2. In contrast to the theoretical expectations, the β values are the same, within tlie experimental errors, for all the three homologues. Thus one can conclude that the experimentally observed features are not brought about by any changes in β and hence tlie bilinear to biquadratic coupling effects.

In figures **3.23** and **3.24** we present the results of $\Delta\epsilon_s$ and f_s for the three homologues. Notice that, in contrast to GM frequency f_G, both $\Delta\epsilon_s$ and f_s monotonically increase with increasing chain length without any odd-even behaviour.

3.3.7 Determination of Landau coefficients by dielectric method

In this section, we present a novel method of determining Landau coefficients by analysing the dielectric data of the soft mode and Goldstone mode for the compound C_6 described in the previous sections. The soft mode viscosity (γ_s) is also calculated and seen to be influencing the thermal variation of f_s.

Table 3.2

Values of P*,θ* and β

for the three homologues of the C_n series

Compound	P* (Cm^{-2})	θ* (rad)	β
C_6	3.1×10^{-3}	0.66	0.53
C_7	1.6×10^{-3}	0.54	0.51
C_8	1.3×10^{-3}	0.48	0.50

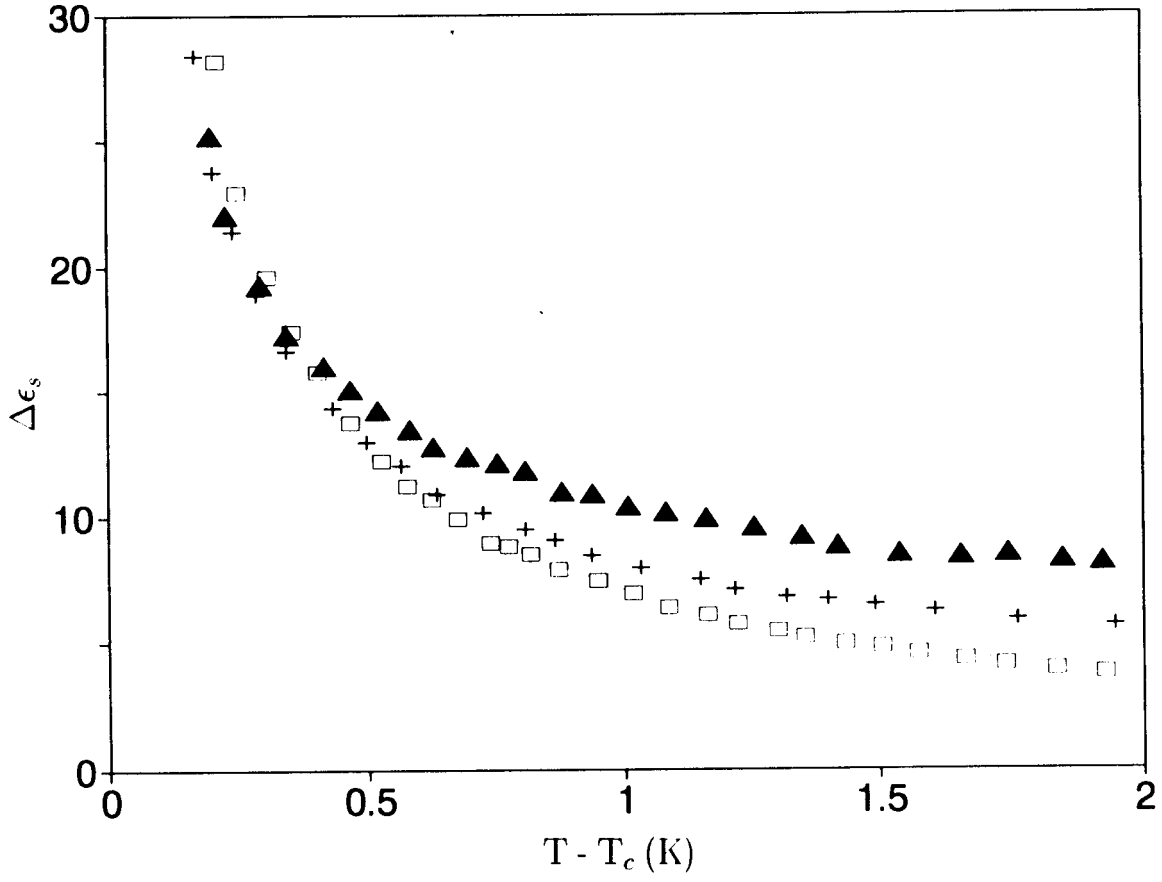

Fig.3.23. Temperature dependence of $\Delta\epsilon_s$ for C_6 (□), C_7 (+) and C_8 (▲)

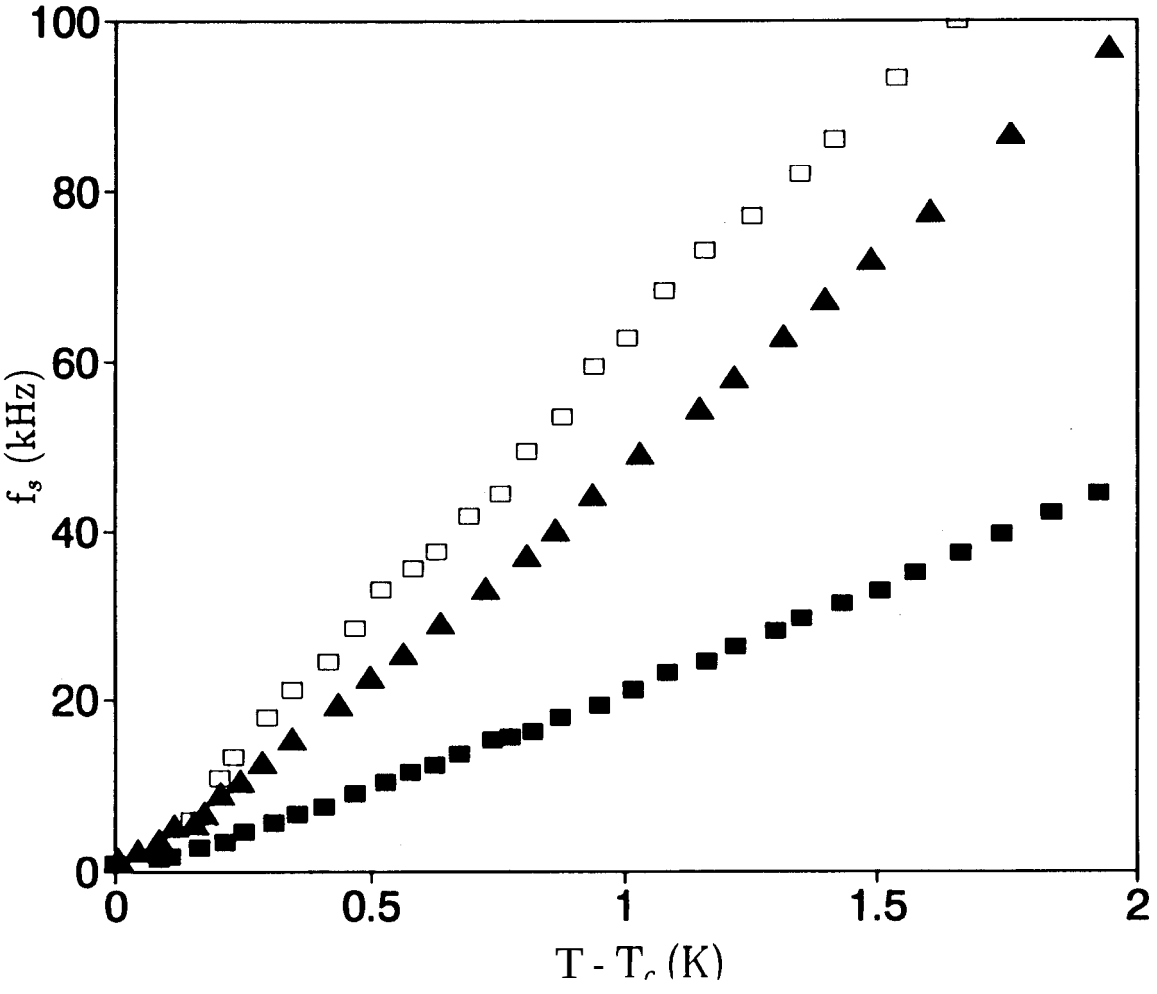

Fig.3.24. Temperature dependence of f_s for C_6 (■), C_7 (A) and C_8 (□).

Figures *3.25* and ***3.26*** show the temperature variation of f_s and **Ac,** for the compound C_6. Since this mode is associated with the order parameter fluctuations (in this case tilt fluctuations), the pretransitional critical behaviour of f_s and $\Delta\epsilon_s$ are governed by the tilt susceptibility exponent γ wtiose value is 1.0 in the mean field (MF) limit and *1.315* if the transition belongs to XY universality class. Tilt angle[**] and heat capacity[43] measurements have shown that this transition is MF like. Early work on the electroclinic effect by Garoff arid Meyer[26] gave a value of 1.11 for tlie susceptibility exponent, which is inconsistent with either MF or XY class values. However more recent measurements[44,45] are in agreement with the mean field description. With tliis in mind, we have fitted the f_s and $\Delta\epsilon_s$ versus temperature data to power law equations of the type

$$f_s = constant \times (T - T_c)^{\gamma} \tag{3.20}$$

$$\mathbf{Ac,} = constant\ \mathbf{x}\ (T - T_c)^{-\gamma} \tag{3.21}$$

Equations *(3.20)* and *(3.21)* appear to describe the data well (solid lines in figures *3.25* and *3.26)* but tlie exponents obtained, *1.19* and 0.88 for f_s and $\Delta\epsilon_s$ respectively, are different from the MF value of *1.0.* In order to understand this discrepancy, we consider eqns. *(3.S)* arid *(3.9)* given by generalized mean field model arid instead of assuming the exponents to be equal to 1, introduce two unknown constants γ_1 and γ_2 as tlie exponents and write the equation as

$$f_s = \frac{1}{2\pi\eta_s}[a(T - T_c)^{\gamma_1} + K_3 q_o^2] \tag{3.22}$$

$$\epsilon_o \Delta\epsilon_s = \frac{(\epsilon_o \epsilon C)^2}{a(T - T_c)^{\gamma_2} + K_3 q_o^2} \tag{3.23}$$

In these equations tlie term $\epsilon\mu^2$, which is known to be very small[46] compared to K_3 has been neglected. From equation *(3.22)* we see that for f_s to be linear

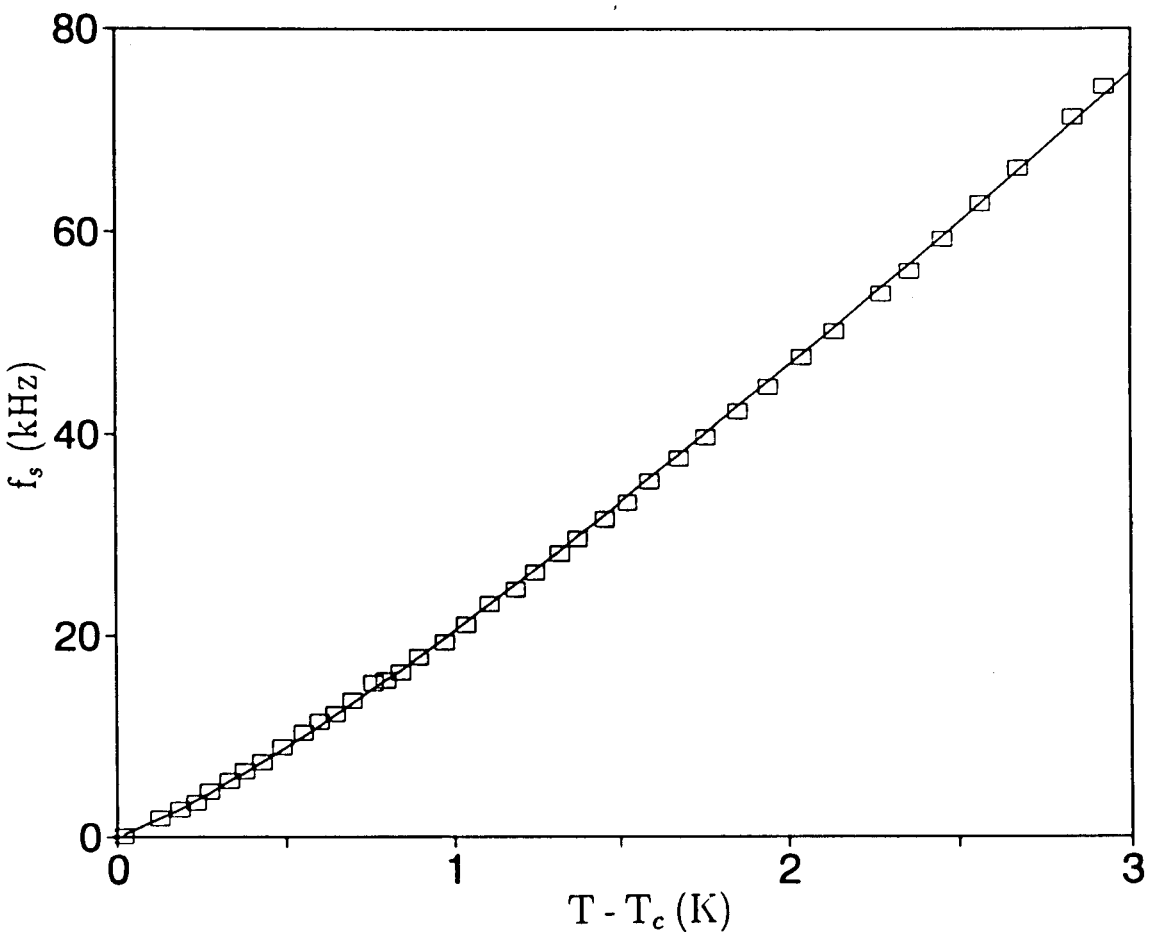

Fig.3.25. Temperature variation of the soft mode relaxation frequency f_s for C_6. (□) data, and (---) fit to eqn. 3.20.

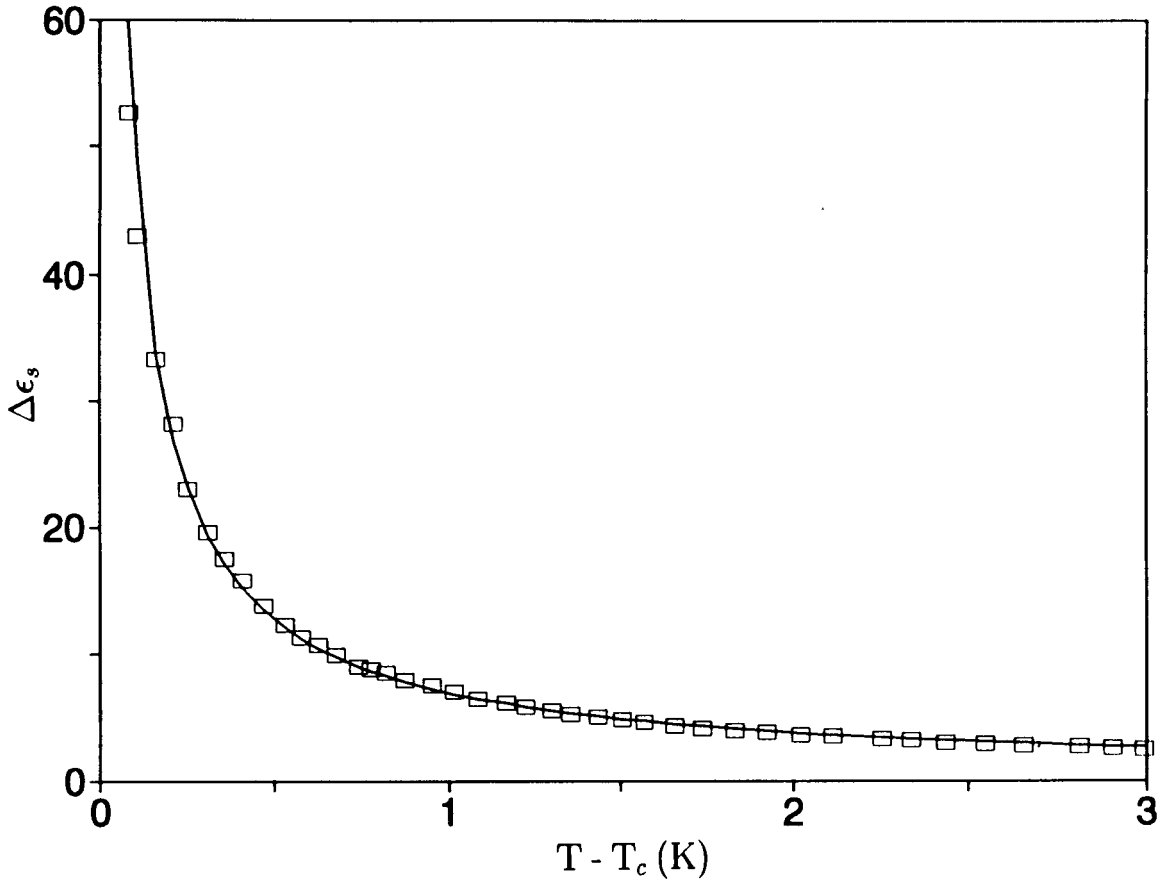

Fig.3.26. Thermal variation of the soft mode strength $\Delta\epsilon_s$ for C_6. (□) data and (—) fit to eq. 3.21.

with temperature (with $\gamma_1 = 1$), η_s should have no or very weak temperature dependence. But experiments indicate that η_s is temperature dependent. Hence in the absence of information regarding the temperature dependence of η_s the exponent γ_1 cannot he extractetl from eqn. (3.22). However, the $\Delta\epsilon_s$ data will riot liave such a constraint. Equation (3.23) can he rewritten as

$$\frac{1}{\Delta\epsilon_s} = A(T - T_c)^{\gamma_2} + B \tag{3.24}$$

where

$$A = \frac{a}{\epsilon_o(\epsilon C)^2} \quad and \quad B = \frac{K_3 q_o^2}{\epsilon_o(\epsilon C)^2} \tag{3.25}$$

Figure 3.27 shows the fit to eqn. (3.24). It is seen that this expression describes the data extremely well (solid line in tlie figure) and the exponent obtained (0.97) is very close to the mean field value. One major advantage of employing eqn. (3.24) is that the constants A and B can be used to calculate tlie Landau coefficients a and C and the SM viscosity η_s. For this purpose, we proceed as follows.

The eqn. (3.12) for GM, can be rewritten as

$$K_3 q^2 = \frac{1}{2\epsilon_o \Delta\epsilon_G}\left(\frac{P}{\theta}\right)^2 \tag{3.26}$$

The value of $K_3 q^2$ has been determined by measuring the thermal variation of Γ and θ (see figures 3.28 and 3.29) and using the $\Delta\epsilon_G$ data (figure 3.21). This is plotted as a function of temperature in figure 3.31. In order to liave an independent confirmation, we liave also used eqn. (3.13) to calculate the value of $K_3 q^2$ as

$$K_3 q^2 = 2\pi\, \eta_G\, f_G \tag{3.27}$$

η_G has been obtained by tlie Diamant method[41] (described in Chapter IV). This method gives η_ϕ, the viscosity associated with the motion of the molecule

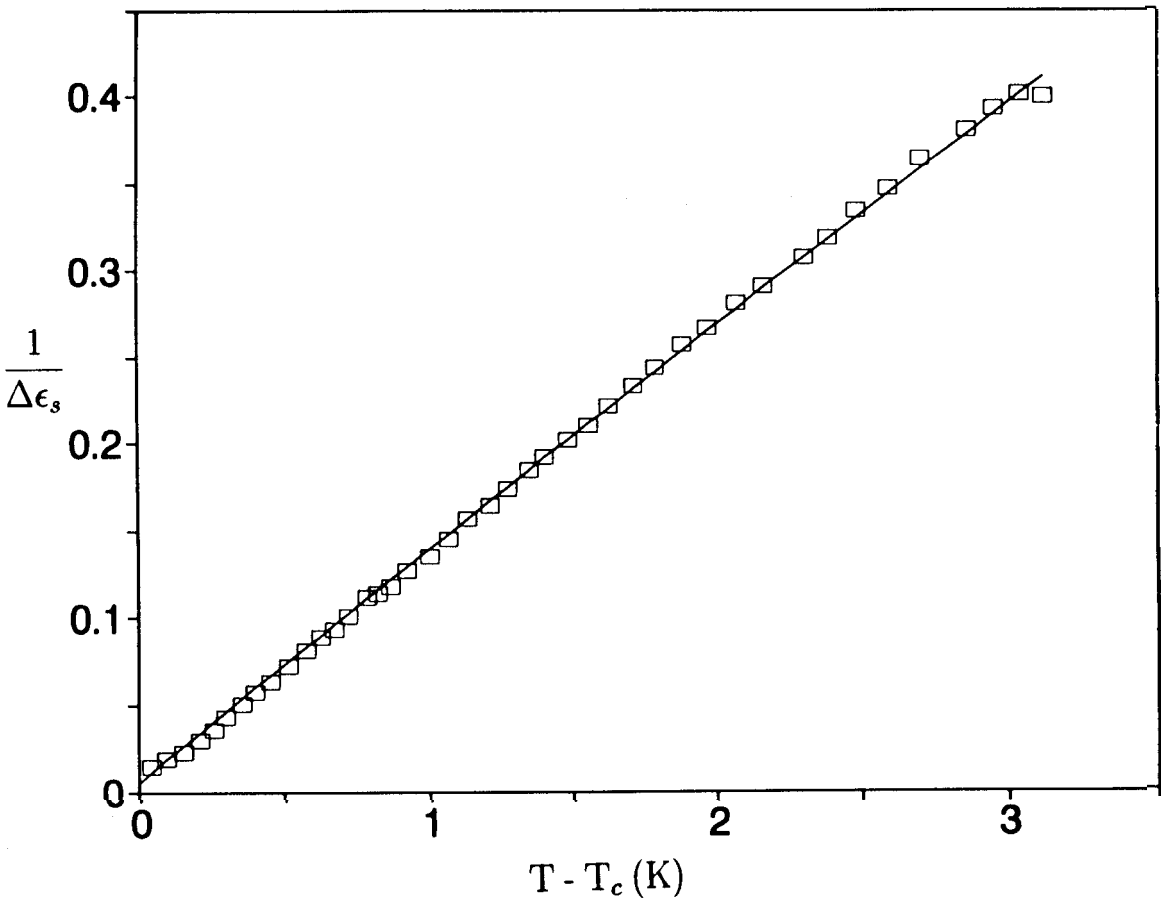

Fig.3.27. Fit of $\frac{1}{\Delta\epsilon_s}$ to eqn.3.24. (□) data (—) fit.

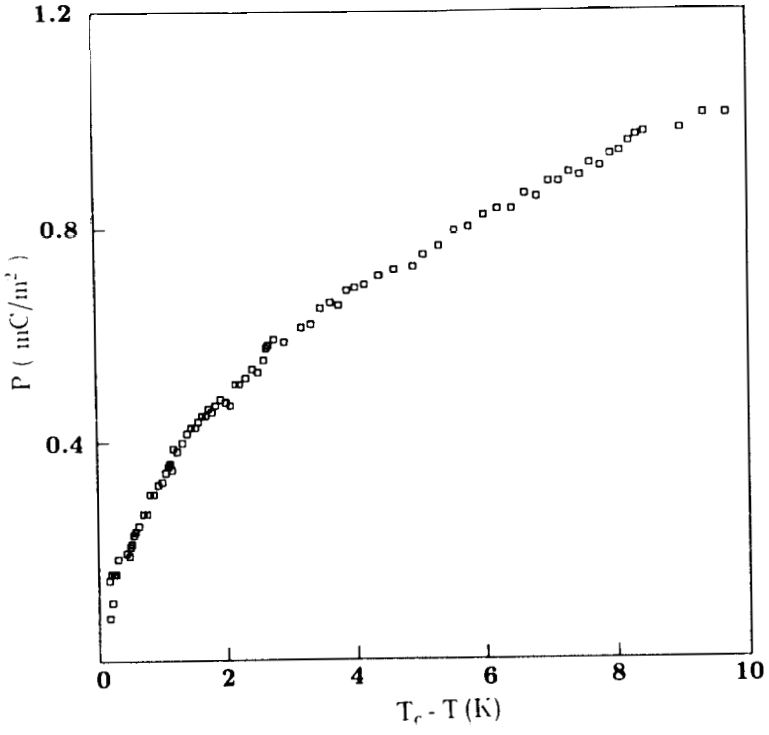

Fig.3.28. Temperature dependence of P_s for C_6.

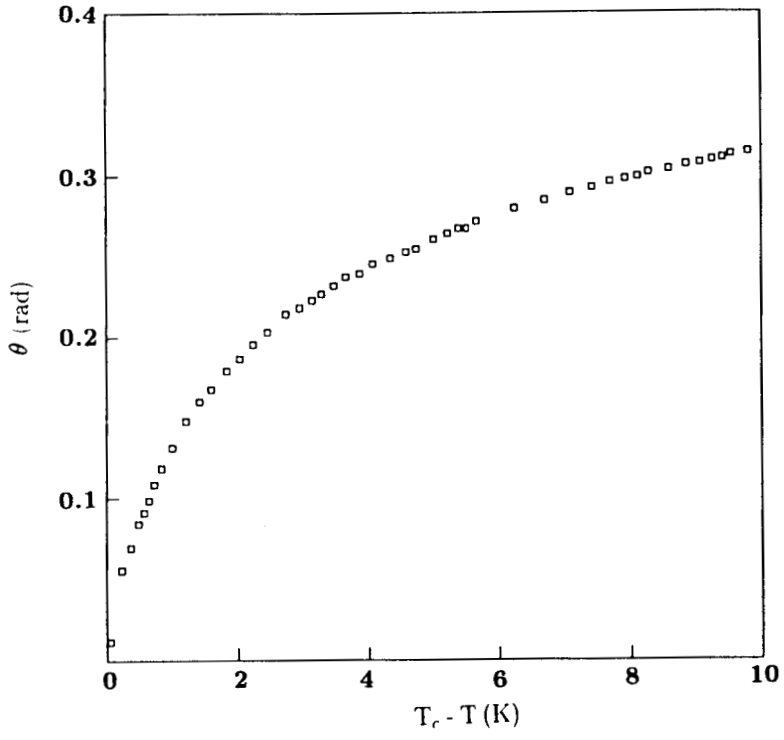

Fig.3.29. Temperature variation of tilt angle for C_6.

around the smectic C cone. The thermal variation of η_ϕ is given in figure 3.30. This semi-log plot shows that away from T_c, η_ϕ has arrlienius type of behaviour but deviates significantly from it on approaching T_c. However, η_ϕ is only an effective viscosity arid the relevant viscosity of interest in present case is η_G, given by[47]

$$\eta_G = \eta_\phi / \sin^2\theta \qquad \textbf{(3.28)}$$

A plot of η_G as a function of temperature is also shown in figure 3.30. It is observed that η_G shows arrhenius behaviour over the entire temperature range of measurements.

Figure 3.31 shows the temperature dependence of K_3q^2 calculated from both eqns. (3.28) and (3.29). Note tliat three different kinds of measurements P_s, X-ray tilt angle and dielectric methods are involved in the calculations arid the K_3q^2 values obtained using the two equations differ by less than 5% throughout the temperature range of measurement. The extrapolated value of K_3q^2 at T_c yields $K_3q_o^2$. Substituting this in the expressions for A arid B, we get,

$$C = (\frac{K_3q_o^2}{\epsilon_o\epsilon^2 B})^{1/2}$$

and

$$a = \frac{A}{B}K_3q_o^2.$$

Tlie values of a and C obtained are given in table 3.3 and are comparable to tlie values $a = 0.89 \times 10^5$ and $C = 0.86 \times 10^8$ got[48] from electroclinic tilt angle measurements on MCP7OB, a compound with high value of P_s.

Knowing the value of C from eqns. (3.32) and (3.23) tlie SM viscosity value

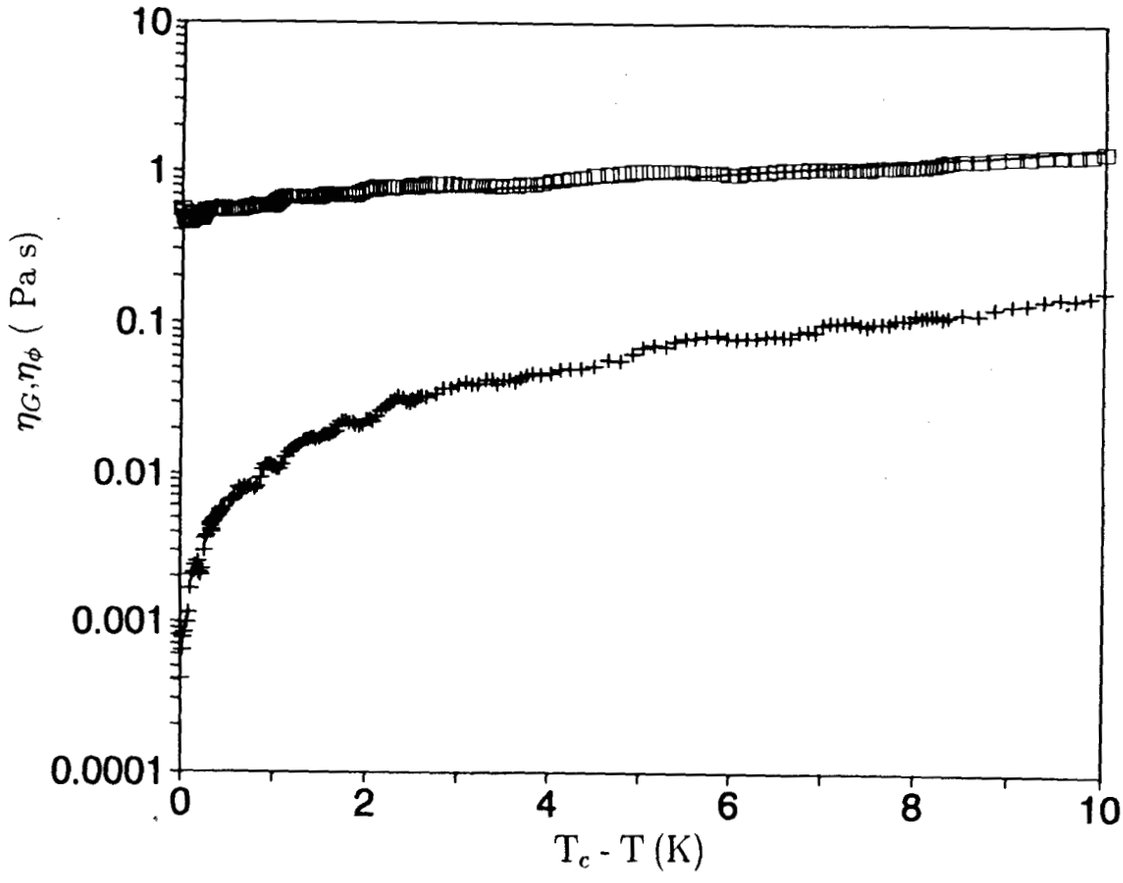

Fig.3.30. Variation of η_ϕ (+) and η_G (□) as a function of temperature. Note that η_G remains Arrhenius right up to the transition.

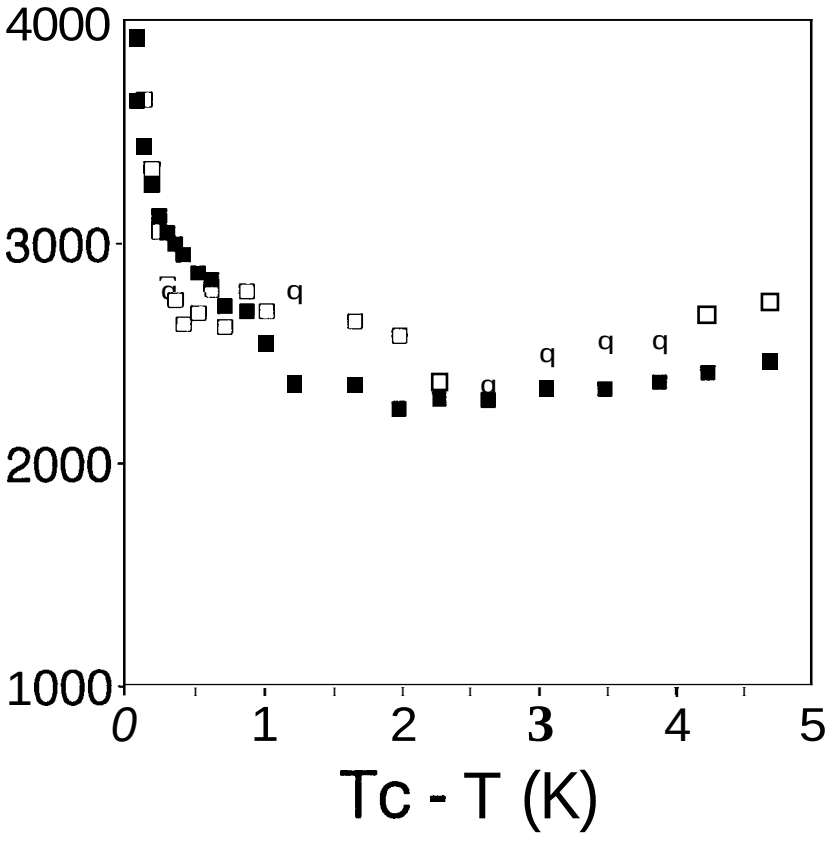

Fig.3.31. Variation of K_3q^2 as a function of temperature, (■) values obtained from eqn. (3.26) and (□) obtained from eqn.(3.27).

Table 3.3

Exponents and Landau coefficients obtained for C_6

Exponent y (from f_s fit)	1.19
γ_2 (from $1/\Delta\epsilon_s$ fit)	0.97
$\gamma - \gamma_2$	0.22
Exponent x (from η_s fit)	0.27
$K_3 q_o^2$	4300 Nm^{-2}
ϵ	3.03
a	1.24 x 10^5 $Jm^{-3}K^{-1}$ rad^{-2}
C	1.07 × 10^8 JC^{-1} m^{-1} rad^{-1}

η_s can be extracted rising tlie relation

$$\eta_s = \frac{\epsilon_0(\epsilon C)^2}{2\pi\Delta\epsilon_s f_s}$$

in the limit of $\gamma_1 = \gamma_2 = \gamma = 1$.

The temperature variation of η_s is shown in figure **3.32.** We have tried to express η_s data by a power law type of equation considering the usual arrlienius background contribution by an equation of tlie form

$$\eta_s = A(T - T_c)^x + \eta_o exp(\frac{B}{T})$$

Here A arid B are constants and tlie second term on tlie R.H.S represent the arrhenius background contribution. This expression fits tlie data well with x = -0.27, which is in fair agreement with tlie value of -0.25 obtained[37] for another compound. Earlier, by considering η_s to be independent of temperature, the exponent for tlie thermal variation of f,, γ was found to be 1.19 which is much higher than the mean field value of 1. However, from eqn. (3.23), where the GMF relation for $\Delta\epsilon_s$ was considered, we got $\gamma_2 = 0.97$. Significantly, the difference between y and γ_2 (= 0.22) is approximately tlie same as tlie value x obtained. Thus the divergence in η_s on approaching tlie transition appears to be largely responsible for tlie difference between tlie exponents γ and γ_2.

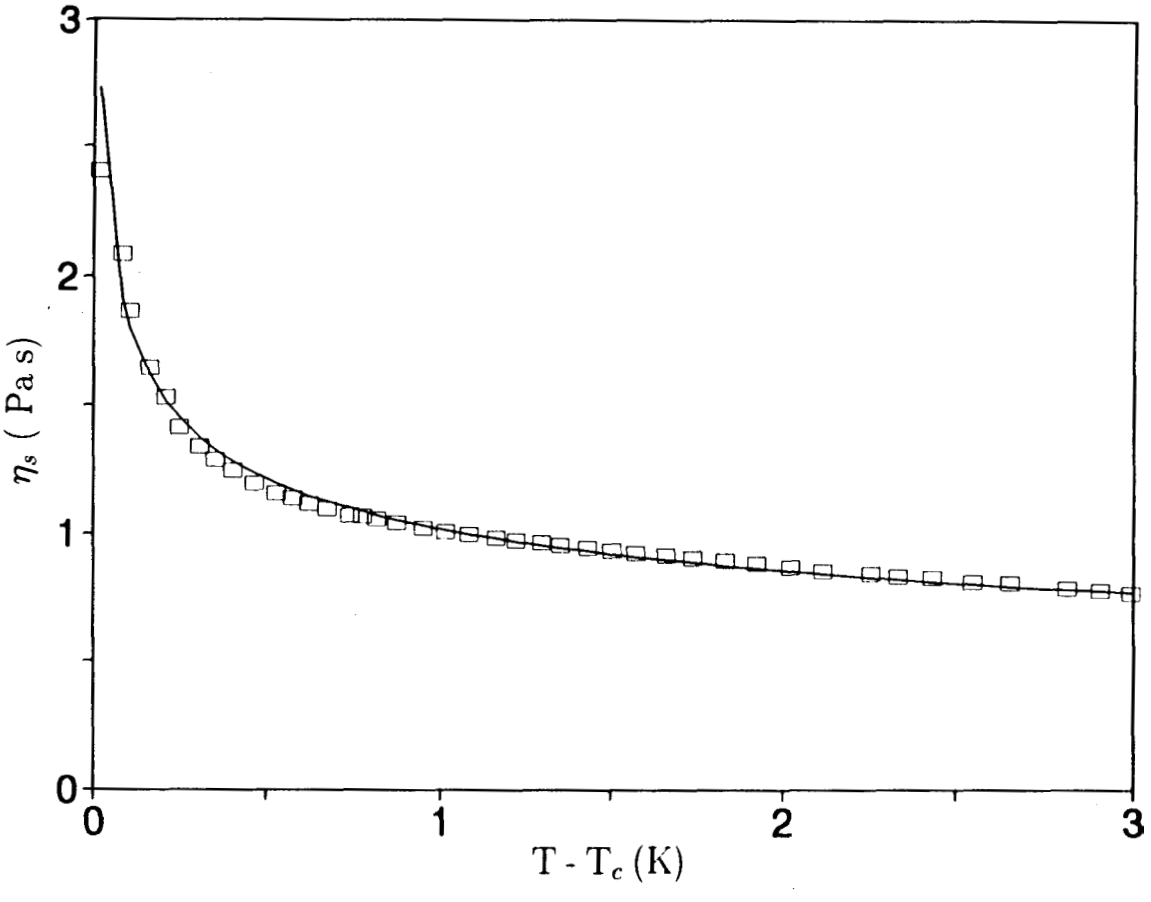

Fig.3.32. Soft mode viscosity η_s variation as a function of temperature. (□) data and (—) fit to a simple power law.

References

[1] P.Debye, Polar *Molecules* (Chemical Catalogue Co., New York 1929).

[2] N.E.Hill, A.H.Price and M.Davies, *Dielectric Properties and Molecular Behaviour* (Van Nostrand Reinhold Co., London, 1969).

[3] B.R.Ratna, *Dielectric Properties and Short* Range *Order in* Liquid *Crystals*, Ph. D. Thesis, University of Mysore (1978).

[4] C.Nagabhushan, *Experimental* Studies on the Dielectric Properties *of* Liquid *Crystals*, Ph. D. Thesis, University of Mysore (1988).

[5] A.Buka and L. Bata, *Mol. Cryst.* Liquid *Cryst.Lett.*, 49, 15'3 (1'379).

[6] R.B.Meyer, *Mol.* Liquid *Cryst.*, 40, **33** (1977).

[7] K.Yoshino, T.Uemoto and Y.Inuishi, *Jap.J.Appl. Phys.*, 16, 571 (1977).

[S] B.I.Ostrovskii, A.Z.Rabinovich, A.S.Sonin and E.A.Strukov, *Sov. Phys. JETP*, 47, 912 (1978).

[9] J.Hoffman, W.Kuczynski and J.Malecki, *Mol. Cryst. Liquid Cryst.*, **44**, 287 (1978).

[10] A.Levstik, B.Zeks, I.Levstik, R.Blinc and C.Filipic, *J. Phys.*, **40**, C3-303 (1979).

[11] D.S.Parmar and Ph. Martinot-Lagarde, *Ann. Phys.*, **3,** 275 (1978).

[12] J.Pavel, M.Glogarova and S.S.Bawa, *Ferroelectrics*, **76**, 221 (1987).

[13] N.Mayurama, *Ferroelectr*ics, 58, 187 (1984).

[14] L.G.Benguigui, *Ferroelectrics*, **58**, 269 (1984).

[15] K.Yoshino, M.Ozaki, H.Agawa and Y.Shigeno, *Ferroelectrics*, **58**, 283 (1984). *Cryst.*

[16] R.J.Cava, J.S.Patel, K.R.Collen, J.W.Goodby arid E.A.Rietman, *Phys. Rev.*, A35, 4378 (1987).

[17] C.Filipic, T.Carlsson, A.Levstik, B.Zeks, R.Blinc, F.Gouda, S.T.Lagerwall arid K.Skarp, *Phys.* Rev., A38, 5833 (1988).

[18] Ch. Bahr, G.Heppke and N.K.Sharma, Ferroelectrics, 76, 221 (1987).

[19] F.Gouda, G.Anderson, T.Carlsson, S.T.Lagerwall, K.Skarp, B.Stebler, C.Filipic, B.Zeks and A.Levstik, *Mol. Cryst. Liquid Cryst.* Lett., 6, 151 (1989).

[20] S.U.Vallerien, F.Kremer, H.Kapitza, R.Zentel and W.Frank, *Phys.* Lett., **A138**, 219 (1989).

[21] T.Carlsson, B.Zeks, A.Levstik, C.Filipic, I.Levstik and R.Blinc, *Phys. Rev.*, A36, 1484 (1987); T.Carlsson, B.Zeks, C.Filipic, A.Levstik and R.Blinc, *Mol. Cryst. Liquid Cryst.*, 163, 11 (1988).

[22] S.Dumrongrattana and C.C.Huang, *Phys. Rev. Lett.*, 56, 464 (1986).

[23] F.Gouda, K.Skarp and S.T.Lagerwall, Ferroelectrics, 113, 165 (1991).

[24] A.H.Price and A.Buka, *Advances* in Liquid Crystal Research *and* ***Applications***, Vol. 1, Ed. L. Bata (Pergamon Press, 1980), p. 267.

[25] R.Blinc and B.Zeks, *Phys. Rev.*, A18, 740 (1978).

[26] S.Garoff and R.B.Meyer, *Phys. Rev. Lett.*, **38**, 848 (1977).

[27] A.Levstik, T.Carlsson, C.Filipic, I.Levstik and B.Zeks, *Phys.* Rev., A35, 3527 (1987).

[28] C.V.Raman and T.M.K.Nedungadi, *Nature,* **145**, 147 (1940).

[29] M.Delaye and P.Keller, Phys. *Rev.* Lett., 37, 1065 (1976).

[30] J.Goldstone, *Nuovo Cimento*, 19, 154 (1961).

[31] S.A.Pikin arid V.L.Indenbom, *Sov. Phys.-Usp.*, 21, 487 (1'378).

[32] T.Carlsson, B.Zeks, C.Filipic and A.Levstik, *Phys. Rev.*, **A42**, 877 (1990).

[33] Th. Martinot-Lagarde and G.Durand, **J.** *Physique*, 41, L-43 (1980) arid ibid, 42, 269 (1981).

[34] K.S.Cole and R.H.Cole, *J. Chem. Phys.*, **9,** 341 (1941).

[35] I.Drevensic, I.Musevic arid M.Copic, *Phys.* ***Rev.,*** A41, 923 (1990).

[36] Ch. Bahr and G.Heppke, *Liquid Crystals*, **2**, 825 (1987).

[37] F.Gouda, K.Skarp, G.Andersson, H.Kresse and S.T.Lagerwall, *Jpn.* **J.** *Appl.* Phys., 28, 1987 (1989).

[38] C.Legrand and J.P.Parneix, *J.Phys. France*, 51, 787 (1990).

[39] J.Pavel and M.Glogarova, *Ferroelectrics*, **84**, 241 (1988).

[40] K.Kondo, H.Takazoe, A.Fukuda and E.Kuze, *Jpn. J. Appl. Phys.*, **21**, 224 (1982).

[41] C.Escher, H.R.Dubal, W.Hemmerling, I.Muller, D.Ohlendorf and R.Wingen, *Ferroelectrics,* 84, 89 (1988).

[42] R.Shashidhar, B.R.Ratna, G.G.Nair, S.Krishna Prasad, Ch. Bahr and G.Heppke, *Phys. Rev.* Left., 61, 537 (1988).

[43] C.C.Huang, *Mol. Cryst. Liquid Cryst.*, 144, 1 (1987).

[44] R.Qiu, J.T.Ho and S.K.Hark, Phys. Rev., A38, 1653 (1988).

[45] Z.Li and C.Rosenblatt, *Phys.* ***Rev.,*** **A39,** 1594 (1989).

[46] See for e.g., T.Carlsson, B.Zeks, C.Filipic, A.Levstik and R.Blinc, Mol. *Cryst. Liquid Cryst.*, **163,** 11 (1988). In this paper it was shown that for DOBAMBC, the $c\mu^2$ value is at, least two orders of magnitude smaller than K_3.

[47] A.Levstik, Z.Kutnjak, C.Filipic, I.Levstik, Z.Bregar, B.Zeks and T.Carlsson, *Phys. Rev.*, **A42**, 2204 (1990).

[48] Ch. Bahr, G.Heppke and B.Sabaschus, *Ferroelectrics*, 84, 103 (1988).